INDIVIDUAL
Faculty of Engineering
Coursework Front Sheet

Family Name	Mantar
Forename(s)	Burcu
Student ID	4218046
Personal Tutor	Dr Edward Christopher

H54MSP

Department	Electrical and Electronic Engineering [E3]	Course	H697
Module Title	MSc Project		
Module Convenor	Dr Arthur Williams		
Assignment Title	**Final MSc Project**		
Date of Laboratory		Lab/WS/Design Group No	
Submission Deadline	**08 September 2014**		

If you have Extenuating Circumstances that you wish to be considered for this coursework, please complete and submit the relevant form to the Engineering Student Support Centre within 7 working days of the submission deadline.
Further information about Extenuating Circumstances is available at:
http://www.nottingham.ac.uk/academicservices/qualitymanual/assessment/extenuatingcircumstances.aspx

Completed Form Submitted	Yes / No	Date Submitted	
Supporting Documentation Submitted	Yes / No	Date Submitted	

Note: ECFs will not be actioned until supporting evidence has been supplied

ALL COURSEWORK MUST BE SUBMITTED TO THE ENGINEERING STUDENT SUPPORT CENTRE IN THE ENGINEERING & SCIENCE LEARNING BUILDING BY 3:00 pm ON THE DATE GIVEN.

Work handed in after this time will be penalised by a deduction of 5% absolute per University working day.

Feedback from Marker [ ] If ticked, feedback on this work is indicated on the body of the work

What has been done well
Suggestions for improvement Please continue on the reverse of the sheet if needed.

Marker's name			Marker's Signature		
Coursework Mark		Deduction for Late Submission		OVERALL MARK	

Marks are provisional until confirmation at the External Examination Board meeting.

Plagiarism (copying, cheating)

In signing this form you are confirming that you have read and understood the University regulations relating to plagiarism and that the content of this document is your own work and has not been plagiarised. Full details of the University's policy can be found at: http://www.nottingham.ac.uk/academicservices/qualitymanual/assessment/academicoffences.aspx

Signature of Student_____ Date: _____

b

The University of Nottingham
UNITED KINGDOM · CHINA · MALAYSIA

DEPARTMENT OF ELECTRICAL & ELECTRONIC ENGINEERING

Coordinated Control of a Large Offshore Wind Farm and a HVDC Link

Author: BURCU MANTAR

Supervisor: Professor Dave Thomas

Date: 8 September 2014

Project thesis submitted in part fulfillment of the requirements for the degree of **Master of Science in Electrical Engineering**, The University of Nottingham

ACKNOWLEDGEMENTS

This master thesis is carried out in the Department of Electrical Engineering for Sustainable and Renewable Energy at the University of Nottingham.

I would like to express my gratitude to my supervisor, **Professor Dave Thomas** for his generous support and professional guidance. Without his helps, this thesis would not be possible to finish. His criticisms and advices had been very beneficial all throughout my thesis.

I would also like to thank **Dr. Arthur Williams** and **Dr. Edward Christopher** for their worthful comments and advices during my master program.

Special thanks are for my PhD demonstrator **Mr. Preye Ivry** of the Nottingham University for his skillful guidance, encouragement and patience all throughout my thesis.

I would like to thank to **Res. and Teach. Asst. Tayfun Gundogdu** who supported me to deal with challenges when I got stuck and also thank to him for worthful comments, advices and endless love.

I owe my deepest gratitudes to my parents, **Tahsin Mantar**, **Birgul Mantar** and my brother **Tayfun Mantar** for their continuous support which I always felt.

Coordinated Control of a Large Offshore Wind Farm and a HVDC Link

ABSTRACT

Owing to the recent developments in semiconductor devices and control equipment, a voltage source converter based high voltage direct current (VSC-HVDC) becomes a significant technology for large offshore wind farms. The VSC-HVDC provides numerous potential benefits over the conventional HVDC such as independent and rapid active and reactive power control and black start capability.

In this thesis, the coordinated control of a large offshore DFIG based wind farm with VSC based HVDC link is investigated. A suitable control strategy for the VSC-HVDC link is devised that ensures the power can be transmitted to the grid despite the variability of the wind farm generated power. This thesis analyses a non-switching average value model of a VSC with its operation at grid side and farm side for load conditions and voltage variations. The non-switching phasor models are adopted in order to model a wind farm with the VSC-HVDC link to the grid.

The main objective of this thesis is to develop Matlab Simulink models of a HVDC link and a wind farm so as to study its control for variations in power flow and fault ride through. In addition, this thesis investigates the complete CIGRE 12 bus bench mark model to demonstrate the performance of the system for load and wind speed variations and for fault conditions.

CONTENTS

Table of Figures

CHAPTER 1: BACKGROUND

Recently, the wind energy application and especially offshore wind energy plays a considerable role for large scale use of renewable energy in the many European countries' policies. Especially, grid connected offshore wind farms has received a major impetus in the country of Sweden, United Kingdom, Germany, Denmark and The Netherlands [1] owing to the global energy consumption growth and the depletion of available fossil fuel reserves [2] [56] [57].

It is the fact that wind energy applications have some demerits such as visual effects and noise. Offshore wind farms provide an ideal solution for these kinds of problems [3]. Therefore, there have been around 53 European offshore wind farms since 1993 and today, the other 10 offshore wind farms are under construction, and this verifies that the use of wind energy to generate electricity will continue to increase [3]. Offshore wind farms provide more advantages compare to onshore due to their larger turbines and rotor blades which cause more electricity generation. In addition, the non-existence of obstacles such as building, mountain and other constructions and stronger wind source on the seashore makes offshore wind farms highly efficient [3].

The first large scale offshore wind farm is Denmark’s Horns Rev, constructed in 2002 with 160 MW capacity. In this project, an offshore transformer substation connected to the shore through a 15-km-long three-core AC cable with 150 kV rated voltage was utilized [1].

The DC power transmission at high voltages and over long distance was possible with the high voltage valves development [4]. There are some important HVDC developments, including Hewitt’s mercury-vapour rectifier (1901), Mercury arc valves in Europe (before 1940), the Gotland 1 in Sweden, the first commercial HVDC transmission, (1954), Argentina-Brazil interconnection, the first capacitor commutated converter (CCC) (1998) and the first voltage source converter for transmission in Gotland, Sweden (1999) [4]. HVDC technology was based

initially on thyristor technology and in recent years on fully controlled semiconductors and voltage-source converter technologies [5]. Today, the fully controlled semiconductor devices are available for high-voltage high power converters and these devices could be utilized for a VSC with pulse-width modulation (PWM) operating at high frequencies and they are all self-commutated through a gate pulse [5]. Comparing to the thyristor-based technology, a VSC application produces higher frequency PWM waveforms although some switching losses which is one of the most series challenge [5].

In today's era, there are around 100 HVDC installations in the world (in planning or in operation) with approximately total 80 GW transmission capacity by employing two distinct technologies, including Line-commutated current–source converters (CSCs) based thyristors and Forced-commutated VSCs based gate turn-off thyristors (GTOs) or Insulated gate bipolar transistors (IGBTs) [5]. The VSC based HVDC technology can be utilized to meet the Grid Code Requirements. It provides wind farm decoupling from the network, which leads to improved Fault Ride-Through capability [6]. In addition, this technology has a growing interest due to providing the independent active and reactive power control and connection of wind farm irrespective to the strength of AC Network [6]. In this thesis, the control strategy of the VSC - HVDC system, which based on vector control is utilized.

1.2 Objective of the Thesis

The main objective of this thesis is to develop MATLAB Simulink models of a VSC based HVDC link and a wind farm so as to study its control variations in power flow and fault ride through and arrive at the best design. A suitable control scheme for the VSC-HVDC link is also devised that ensures the power can be transmitted to the grid despite the variability of the wind farm generated power. The aims of the study are summarized as:

- To construct a non-switching phasor model with suitable control and demonstrate its operation of the farm side voltage sourced converter (FS-VSC) to ensure that the AC voltage can be controlled by the converter independently of the current source amplitude and DC load size.
- To construct a non-switching phasor model with suitable control and demonstrate its operation of the grid side voltage sourced converter (GS-VSC) to ensure that the DC voltage can be controlled by the converter independently of the current source amplitude and DC load size.
- To construct a complete HVDC link by combining the GS-VSC and FS-VSC and demonstrate its action when it's supplied by an AC current source on the farm side.
- To attach the average model of the wind farm to the complete HVDC link using the wind farm data in Appendix and demonstrate the operation of the system under changing wind speeds and for a phase to ground fault on the grid side.
- To construct the complete CIGRE 12 bus bench mark model as seen in Appendix and show the performance of the system for load and wind speed variations as well as for a fault.

1.3 Contribution of the Thesis

The main contribution of this thesis is to study the control strategy for a voltage sourced converter based HVDC link, including the grid side and farm side control.

It is very challenging to model the wind farm and a HVDC link by utilizing its complete models of the switching devices owing to its complexity. A complete DFIG wind farm model with controls is provided in the MATLAB SimPowerSystems toolbox. On the other hand, this thesis presents an average value mathematical model for the voltage source converters, considering that the VSC can

fully control its voltage and there is no power lost in the converters. This report proves the operation of the HVDC link by combining the GS-VSC and the FS-VSC when it is supplied on the farm side by an AC current source and with the phasor model (average model) of the wind farm in respect of its given data. In addition, the operation of the system under variable wind speeds and for a phase to ground fault on the grid side is demonstrated. It can be resulted that the expected coordinated control for the grid fault situation is achieved with the fast responses between the VSC and the average wind farm model and this is very difficult to pursue for the real system design. Hence, this thesis has the prime aim to bring out new methodologies to attain a coordinated control for VSC based HVDC transmission system and DFIG based offshore wind farms in order to perform smooth operation under variable wind speeds and reach fault ride through under grid fault conditions, successfully.

CHAPTER 2: LITERATURE REVIEW

2.1 Introduction of HVDC Transmission System

High Voltage Direct Current (HVDC) is a significantly efficient alternative for large amount of the electricity transmission over long distances for several applications. As an essential enabler in the further renewable energy system, HVDC is considerably shaping the power network of future [7] [54] [55]. HVDC technology was originally developed in Sweden more than 60 years ago. The level of power transmitted has been varying from 40 MW to 8 GW with HVDC system [8]. The HVDC is commonly utilized for the purpose of power transmission to major centers, offshore wind power transmission, dynamically AC networks stabilization and decoupling large AC power networks [8], [9]. The HVDC transmission system is not required reactive power absorption or generation [2]. Therefore, HVDC transmission is highly suitable for over long distance, bulk power delivery, the cable crossing of the long submarine and asynchronous interconnections [10].

The interconnection of regional systems which operate asynchronously could be allowed by HVDC system and this mitigates the issues of instability, otherwise that would lead to outages in AC transmission [11].

There are three generations of HVDC, including Mercury Arc, Thyristor and IGBT technology [11]. Until recently, Classic HVDC based on thyristors was utilized in the conversion of AC to DC and vice versa. In recent years, an innovative HVDC based on advanced semiconductor technology has been used for power conversion. The converters are Voltage Sourced Converters (VSCs) and they could operate with a high switching frequency (1-2 kHz) using Pulse Width Modulation (PWM) and the semiconductors utilized are Insulated Gate Bipolar Transistors (IGBTs) [12]. The technology is commercially called as HVDC Light or HVDC Plus [12]. VSC-HVDC transmission systems have been classified under brand names, including HVDC PLUS (Siemens), HVDC Light (ABB) and HVDC MaxSine (Alstom) [13].

2.2 HVDC versus HVAC Transmission

It is widely accepted that alternating current (AC) is very common for the use of industrial and domestic purposes; however, AC has some limitations which cause the use of DC transmission in many projects [15].

2.3 The Comparison of the Advantages of the HVDC and HVAC Transmission

The benefits of the HVDC and HVAC transmission are compared as given below:

- There are two significant factors for high voltage transmission line, including voltage and current limits. The DC resistance of a conductor is lower than its AC resistance due to skin effect; therefore losses are lower in the DC transmission system [15].
- The losses of an optimized HVDC transmission line are lower than the AC lines for the same capacity of power [16].

- It is true that initial costs of HVDC stations are very high owing to the fact that they have to perform the conversion from AC to DC and DC to AC. On the other hand, according to Figure 2.1, over a certain distance, called “break-even-distance” (600-800 km), a HVDC system becomes costly-effective compare to HVAC system [16].

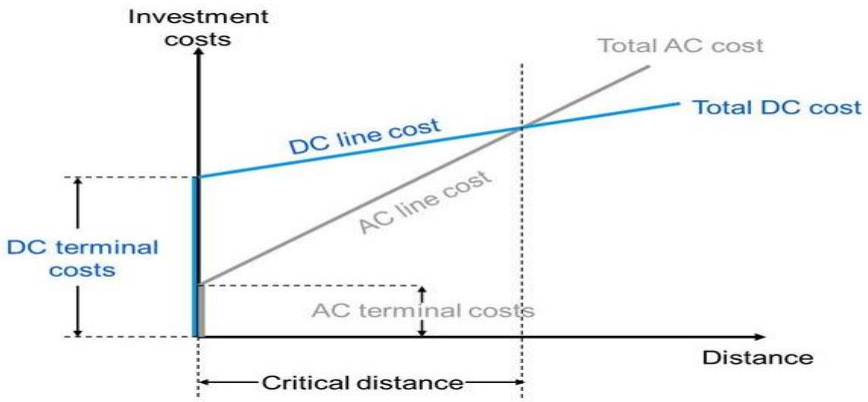

Figure 2.1: Comparison of AC and DC line costs based on break-even distance [16].

- In case of bulk power transmission with submarine and underground cables in long distance, HVDC gives a great performance. In an AC transmission system, the cable resistance leads to reactive power flows, therefore this causes the limitation of transmission distance and additional costs [17]. Moreover, reactive power compensation is required in the AC system. Economic merits and lower line losses make HVDC effective for long distance power transmission [17].
- DC power could be transmitted greater distances than AC power with theoretically no distance limitation [18].
- It is widely accepted that HVDC transmission system is a better alternative for offshore wind farm connection to the grid and power transmission from remote energy resources to large urban areas [17].
- HVDC system provides to link two systems operating at different frequencies or is independent of the two centers relative phases [18].

- In DC systems, overhead line clearances are smaller; this causes smaller rights of way [18].

2.4 Disadvantages of HVDC System

- **Operational Cost:** The cost of power electronics and converter transformers are quite high in a HVDC transmission system construction. To obtain high technical performance in the HVDC system, several components are required [17].
- **Harmonics:** It is true that during the process of conversion, harmonics are produced by electronic converters. A modern HVDC system has several converters, therefore harmonics increase and these effects power electronic devices, power quality and causes system oscillation [17].
- **Grid integration issue:** There is a challenge in the connection of HVDC system and AC system. The large size of AC harmonic filters lead to considerable over voltages in HVDC systems during fault recovery. On the other hand, in power networks, HVDC system shows great performance of the protection of fault [17].
- **Network stability:** It is expected that there will be more HVDC interconnections in power grids. The communication problems between these HVDC schemes might cause instability of the system [17].

2.5 HVDC System Arrangement

HVDC systems could be configured in several ways to meet the operational requirement and provide flexibility [13]. The configuration selection depends on the location and functions of converter stations. Some of the main arrangements are given in Figure 2.2 [19]. A two terminal HVDC system is utilized to transfer power from one place to another as shown in Figure 2.2. In back-to-back HVDC system, the two converters are situated at the same place and the bridges of

the converter are connected directly. A hybrid connection has three or more HVDC substations which are separated by interconnecting transmission lines.

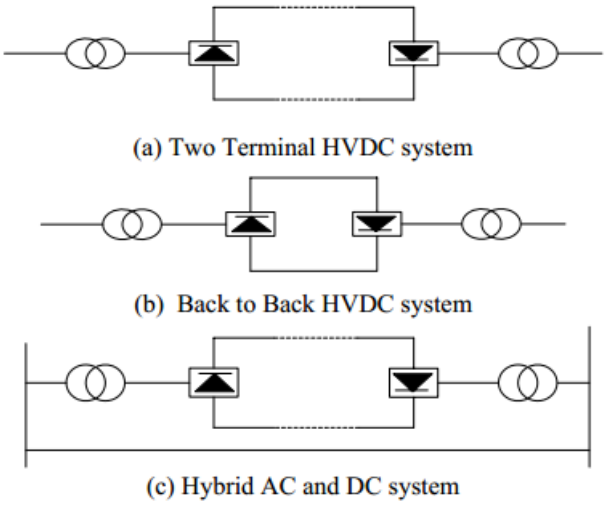

Figure 2.2: Typical AC-DC connection arrangements [19].

2.6 Converter Classification for HVDC Transmission System

The converters used in HVDC system are broadly classified as line-commutated and self-commutated (or forced commutated) depending on the kind of power switching devices applied.

1. **Line-Commutated Converters (CSCs)** based thyristors is shown in Figure 2.3**.** This is well-established technology for the application of high power, generally around 1000 MW, for an instance of this kind of projects is in Brazil with 6300 MW capacity [5].

The main issues of LLC-HVDC Systems [9]:

- Input current has many harmonics which needs filtering in order to not affect transmission network operation which causes the increase of losses and the size of the station [9].
- LLC-HVDC needs an electrical network for its operation. This inability of operation on a “dead network” is a demerit compared to alternatives [9].

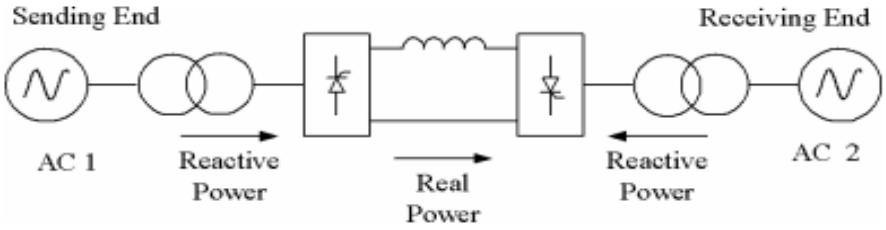

Figure 2.3: HVDC system based on CSC technology [6].

2. **Forced-Commutated (VSCs) Converters** based modern approach using Insulated Gate Bipolar Transistor (IGBTs) is shown in Figure 2.4 [6]**.** Voltage source converter based high voltage direct current system (VSC-HVDC) is the recent development in the field of DC power transmission.

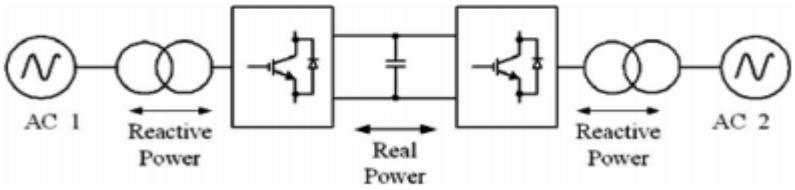

Figure 2.4: HVDC system based on VSC technology [6].

2.7 VSC based HVDC Transmission System

Nowadays, high voltage direct current based on voltage source converters (VSC-HVDC) technology has become feasible due to the recent advancement in semiconductor and control technology [22].

VSC-HVDC is based on the voltage source converter, where the structure of valves consists of IGBTs and PWM which produces the desired voltage waveform [15] PWM could produce any waveform which set by the frequency of switching, fundamental component magnitude and phase angle. By changing the pattern of PWM, it is possible to chance waveform, magnitude and phase angle [15]. As a result of this, the voltage source converter could be considered as a controllable voltage source. The high controllability plays an important role in numerous kinds of application

[15]. Owing to the utilizations of VSC-technology, and pulse width modulation (PWM), VSC-HVDC has a large number of benefits such as independent and rapid reactive and active power control (ability of reactive power absorption/delivery) and the contribution of controllable short-circuit current. As a result of this, VSC-HVDC could be utilized to solve network constraint problem, efficiently, although the increased investment costs and losses depending on the network topology [22].

Typically, a VSC application produces higher frequency PWM waveforms compare to the thyristor-based system. However, these devices' operating frequency is also determined by the losses of switching and the heat sink design, both of them are related to the power through the component [6]. The switching losses depend on high-frequency PWM operation and this is one of the most challenging and serious issue that requires to be handled in VSC-based high power applications [6]. Other considerable demerits that take place by a VSC operation at high frequency are the electromagnetic interference (EMI), high frequency oscillations that need additional filters, and transformer insulation stresses [6].

By comparison with conventional line-commutated HVDC systems, VSC-HVDC systems have several advantages as given follows:

- Both active and reactive power can be controlled independently from each other without additional compensating equipment [23], [24].
- Self-commutation with VSC has "black start" capability- can feed a "dead" network [9].
- It means restoring a power plant to operation without the requirement of external energy sources [25].
- It is possible to obtain dynamic response with excellent results, this is essential to comply with grid code regulations [26].

- VSC-based designs provide superior performance at weak systems (low short circuit ratio application) [27].

On the other hand, the VSC-based HVDC technology has some disadvantages such as high cost and high power losses of the converter stations by comparison conventional HVDC technology [28]. Despite its drawbacks, VSC-HVDC systems are suitable for several applications such as offshore applications, undersea cables and long distance bulk power transmission [29].

2.8 The configuration of a VSC based HVDC Transmission System

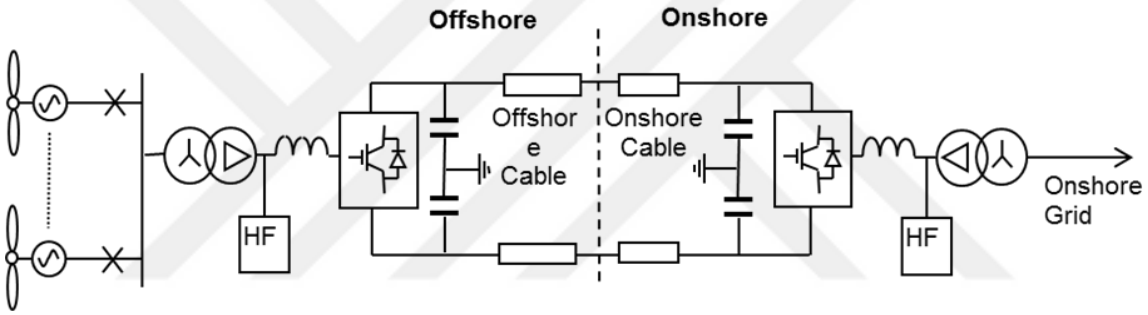

Figure 2.5: A single line diagram of wind farm connected to the grid by a VSC-HVDC Link.

Figure 2.5 shows a typical single line diagram of wind farm connected to the grid by a VSC-HVDC link, consisting of two voltage sourced converters, AC filter, DC link capacitors, DC cable, phase reactor and Doubly- Fed Induction generators. The description of each component of the whole voltage source converter based HVDC system is given below [30]:

Converter Transformer: A power transformer is utilized to change the level of the offshore network voltage to the suitable level for the converter. The ordinary three phase power transformer can be used and a galvanic isolation between the AC side and DC side is provided by this transformation. This is necessary in fault condition in either of the connected parts [31].

AC Filter: Different control scheme can be used for operation of voltage source converters. In most cases, Pulse Width Modulation (PWM) is used for the control of the ratio of the fundamental

frequency voltage through the DC side to AC side. The AC side converter terminal voltage has harmonic components due to the switching of the valve bridge. AC filters prevent these harmonics from passing into the connected AC system. The size of the filter can be between 10 to 30 percent of the rated DC power, depending on the requirements of the filter performance [32].

Voltage Source Converter: A typical VSC utilizes fully-controllable switches such as IGBTs or gate turn-off thyristors (GTOs). Fully-controllable switches are usually used for high power applications with high switching frequencies (2 kHz).The switching devices are usually controlled with PWM techniques to produce a sinusoidal waveform on the AC side and they are filtered by the AC filters and the phase reactor. Therefore, the reproduced waveform harmonic components are maintained low [31]. The IGBTs are arranged in several ways, causing converter topologies. These topologies are commonly classified as two level topology and multilevel topology. The significant aims of these topologies are:

(i) To minimize the switching losses of the semiconductors used in the VSC.

(ii) To generate a high-quality sinusoidal voltage waveform and minimize the filtering requirements [33].

Simple control and power circuitry, small foot print environmentally and small size of DC capacitor are key benefits of the two-level VSC. Figure 2.6 shows a two level three-phase voltage source converter and its p.u voltage waveform.

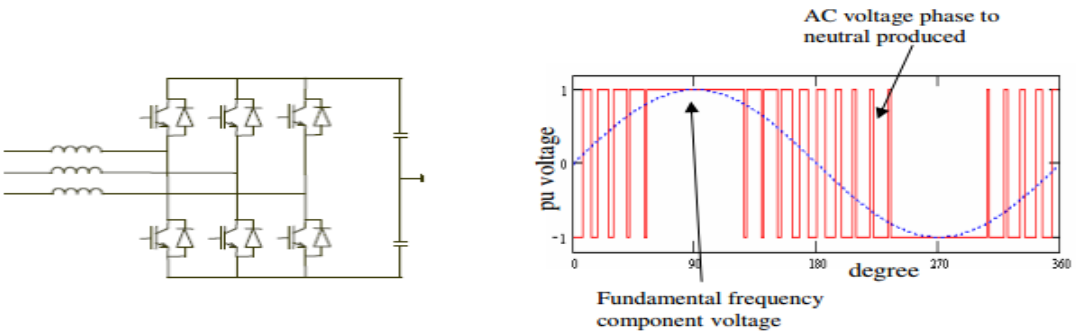

Figure 2.6: Two-level three-phase converter [33].

DC Link Capacitors: The main purpose of the DC capacitors given in Figure 2.6 is to maintain the DC voltage at a constant value. Therefore, the DC capacitor design has a prime importance. The size of a DC capacitor is determined by the time constant τ which defines as a ratio of the DC power stored in the DC link of the converter the apparent power of the converter [33]. **DC Cable:** The recent HVDC cable mostly used is made of extruded polyethylene [34]. **Phase Reactor:** Phase reactors are utilized for the control of both reactive and active power flow by regulating currents between them [30]. **Doubly-Fed Induction Generator:** A Doubly-Fed Induction Generator (DFIG) consists of a wound rotor induction generator and an AC/DC/AC IGBT based PWM converter. The stator winding is directly connected to the grid frequency of $50\ \text{Hz}$, meanwhile the rotor is fed at variable frequency through the AC/DC/AC converter. The DFIG technology provides the maximum energy extraction from wind at low wind speed by optimizing the speed of the turbine [35].

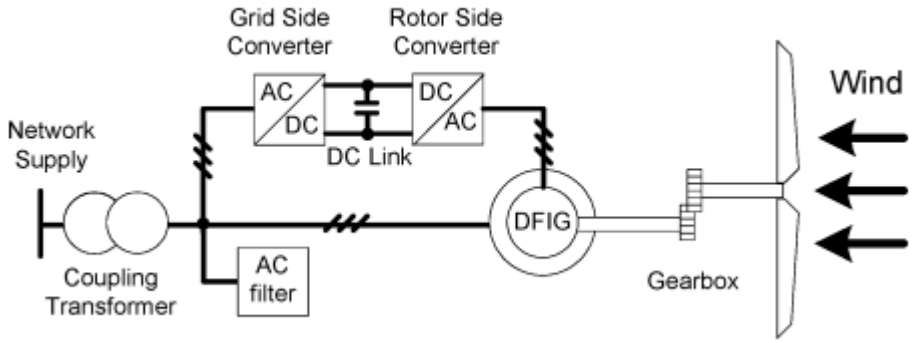

Figure 2.7: A schematic diagram of DFIG based wind turbine [37].

Recently, many wind turbines based on DFIG has been employed in wind farms, because DFIGs offer several merits such as speed control, four-quadrant reactive and active power capabilities, reduced flicker and higher DFIG operating efficiency compare to fixed speed generators [36], [37]. They are mainly achieved via rotor side converter control, which is commonly rated at approximately 30% of the rating of the generator for a given rotor speed variation range of $\pm 25\%$. DFIG based wind turbine schematic diagram is shown in Figure 2.7 [37].

2.9 The Fundamental Concept of a VSC based HVDC Transmission

When voltage source converter is linked to a power grid which is referred as active load, the reactive and active power flow can be controlled independently by changing the amplitude and phase of the AC voltage produced by the voltage sourced converter with respect to the grid voltage [38], [39]. The VSC connected to a power grid gives a performance like a synchronous machine stator as seen in Figure 2.8. This assumption is based on the fundamental frequency component. As a result of this, the reactive and active power flow between generator and active load can be instantaneously controlled by the VSC [39]. The active power (P) and the reactive power (Q) shown in Figure 2.9a flow between the converter and the AC network are calculated as in Eq. (2.1), assuming a lossless reactor at the fundamental frequency [39], [30].

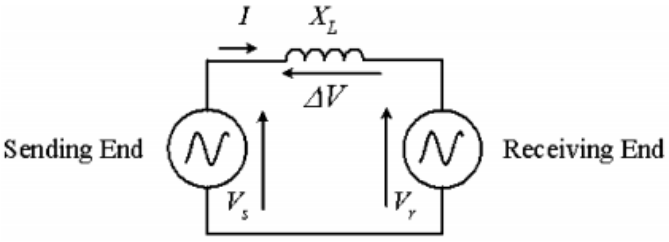

Figure 2.8: The interconnection of two AC voltage sources through a lossless reactor [30].

$$P = \frac{V_S \sin\delta}{X_L} V_R \quad , \quad Q = \frac{V_S \cos\delta - V_R}{X_L} V_R \qquad (2.1)$$

Where V_S is the sending end voltage source, V_R is the receiving end voltage source, δ is the phase angle between the phasor Vs and V_R [30]. Figure 2.9b illustrates the phasor diagram of the V_S and V_R.

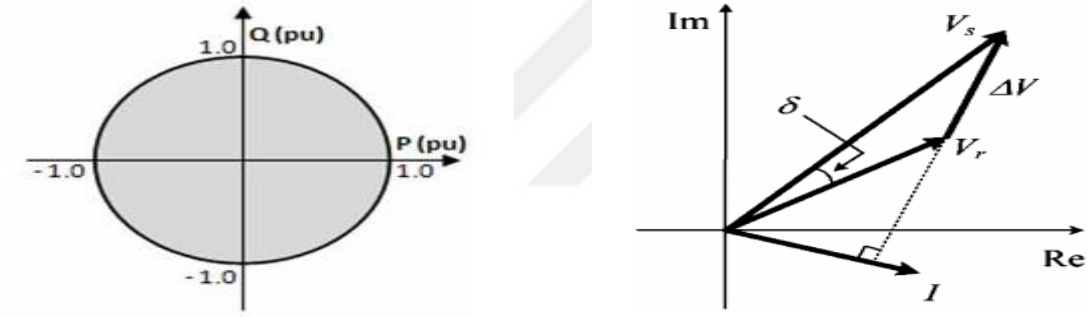

a) b)

Figure 2.9: a) Active-reactive characteristics of a VSC based transmission system [40], b) Phasor diagram of two AC voltage sources interconnected via a lossless reactor [30].

2.10 A Practical Installation of VSC based HVDC Transmission System

Figure 2.10 shows the INELFE Converter stations utilizing the HVDC PLUS Voltage Source Converters. INELFE is the worlds first VSC based HVDC System with 2×1000 MW developed by Siemens. The INELFE/Siemens transmission between Baixas (France) and Santa Liogaia (Spain) is a major component of the trans-European electricity network. The commercial operation of this transmission system is scheduled for 2014. The technical data of INELFE transmission system is shown in Figure 2.10 [41].

Figure 2.10: The INELFE, France-Spain VSC-HVDC Transmission System and its technical data [41].

CHAPTER 3: HVDC LINK MODELLING

This chapter describes a mathematical model of VSC-HVDC system (the average value model). At the next stage, this average value model will be utilized for the VSC based HVDC system control design.

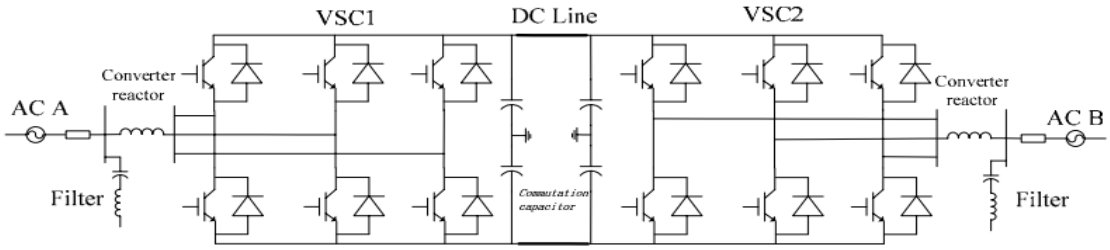

Figure 3.1: The schematic diagram of basic VSC based HVDC [42].

The basic schematic diagram of a VSC-HVDC system is demonstrated in Figure 3.1 [42]. A VSC-HVDC system has two voltage source converters on both DC link ends with the same structure and both connect to AC networks [42]. These converters are operated independently and individually without any communication with each other [43]. Due to its same configuration, the average value model of the both converters should be the same [43]. Figure 3.2 shows the equivalent circuit diagram of VSC-HVDC [44]. For the analysis' simplicity, it is assumed that the system is operated under the balanced condition and there also are no power losses in the

converters. According to the equivalent circuit diagram, $Us[abc]1$ and $Us[abc]3$ are three phase AC infinite sources of rectifier and of the inverter respectively, while $Vs[abc]1$ and $Vs[abc]3$ are three phase AC voltages of the rectifier and of the inverter, respectively [44].

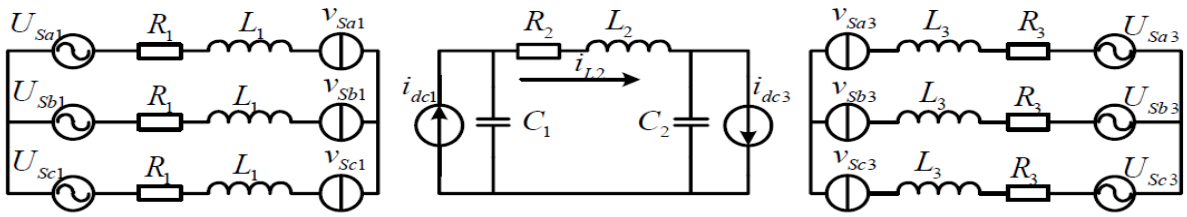

Figure 3.2: The equivalent circuit diagram of a VSC- HVDC [44].

$IL2$ is the DC cables' DC current; $L1, R1$ and $L3, R3$ are the equivalent reactors and resistors of the rectifier and of the inverter, respectively [44]. $L2$ and $R2$ are the equivalent reactors and resistors of DC cables; $C2$ and $C1$ are the DC capacitors of the inverter and of the rectifier, respectively [44].

3.1 Average Value Model

The converter is modelled as a controlled current source Idc on the DC side and a controlled voltage source Uv on the AC side. The non-switching model utilizes ideal voltage sources expressed as in Eq. (3.1) [43]:

$$Vsa = \frac{1}{2}.Vrefa.Vdc \quad , \qquad \mathrm{Vsb} = \frac{1}{2}.Vrefb.Vdc \quad , \qquad \mathrm{Vsc} = \frac{1}{2}.Vrefc.Vdc \tag{3.1}$$

An average model does not represent the switching pattern and therefore, current and voltage values do not have any harmonic content [43]. $Vrefa$, $Vrefb$, $Vrefc$ are the output voltages attained from the control system in which the phase and the amplitude could be controlled independently and they are calculated as in Eq. (3.2) [43]:

$$Vrefa = Ma.\sin(\omega t + \delta),\ Vref\ \mathrm{b} = Mb.\sin\left(\omega t + \delta - \frac{2\pi}{3}\right),$$
$$Vref\ \mathrm{c} = Mc.\sin\left(\omega t + \delta + \frac{2\pi}{3}\right) \quad (3.2)$$

Where Ma, Mb, Mc are the modulation indexes, the ratio between the fundamental peak phase voltage and the DC voltage, and δ is the phase angle of the output voltage [43].

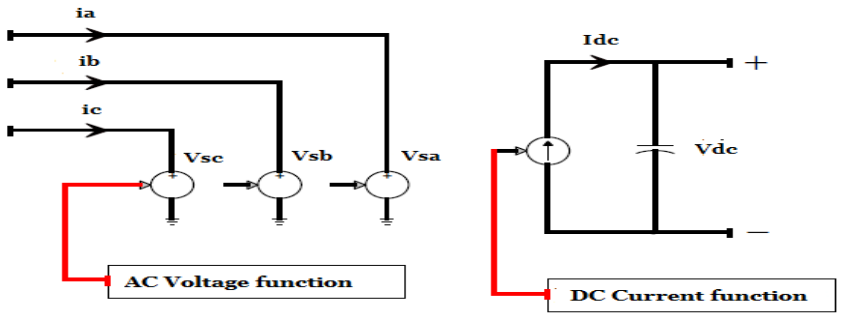

Figure 3.3: Average value model diagram for the VSC [45].

In Figure 3.3, neglecting the losses of the converter, the controlled current Idc on the DC side is given as in Eq. (3.3) [45]. According to Figure 3.2, the dc side of the VSC is obtained utilizing power conversion principle, this means that ac side power must be equal to the dc side power plus power losses. Figure 3.3 shows the average value models, including voltage-controlled sources on the ac side and current controlled sources on the dc side [45]. According to model given in Figure 3.4, the output voltage obtained from the control loop is fed into the VSC. As seen Figure 3.4, the voltages across each phase of the VSC attained from the controller loop are symbolized as $Uconva$,$Uconvb$,$Uconvc$. Therefore, the modulation index M of each phase is calculated as in Eq. (3.4).

$$Uva.ia + Uvb.ib + Uvc.ic = Vdc.Idc \quad (3.3)$$

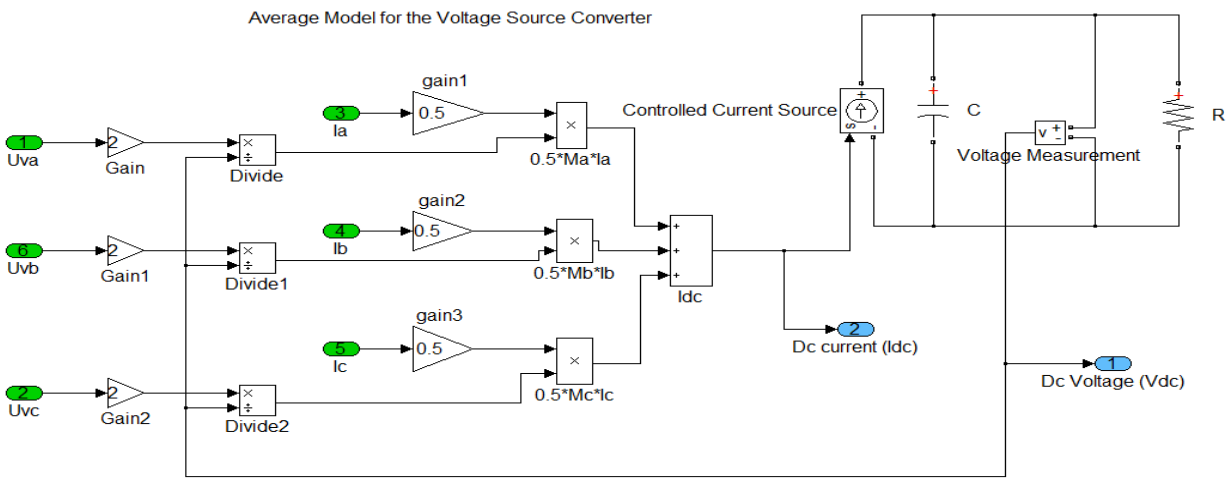

Figure 3.4: Average model for the voltage source converter in Matlab/Simulink.

$$Ma = \frac{2.Uconva}{Vdc} \quad , \quad Mb = \frac{2.Uconvb}{Vdc} \quad , \quad Mc = \frac{2.Uconvc}{Vdc} \tag{3.4}$$

From equation (1.4), the dc current is computed using the measured ac current in each phase as in Eq. (3.5). [43]:

$$Idc = \frac{1}{2}\left(Ma.\mathrm{I}a + Mb.\mathrm{I}b + Mc.\mathrm{I}c\right) \tag{3.5}$$

CHAPTER 4: CONTROL SYSTEM DESIGN

The control strategy of the Voltage Source Converter based HVDC system is presented in this chapter. The Farm Side and the Grid Side Control Strategy for VSC-HVDC transmission system will be explained and the designs of the control loops are also described. The overall control structure of the VSC-HVDC link is shown in Figure 4.1. The most common control strategy for VSC-HVDC system is the vector control methodology [30]. In this thesis, the vector control strategy is used for the control of the VSC based HVDC system.

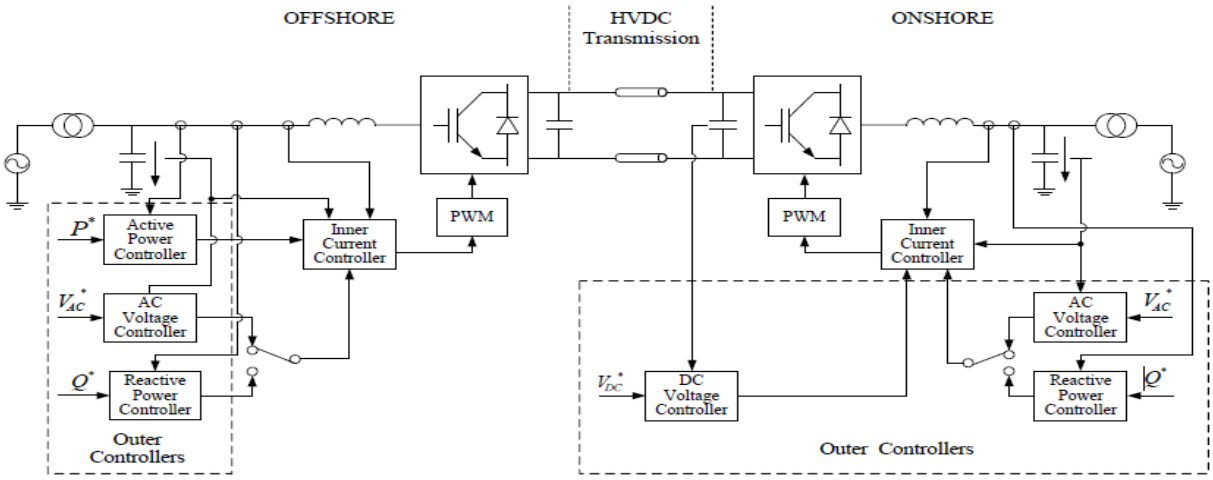

Figure 4.1: The overall control structure of a VSC based HVDC System [30].

4.1 Vector Control Methodology

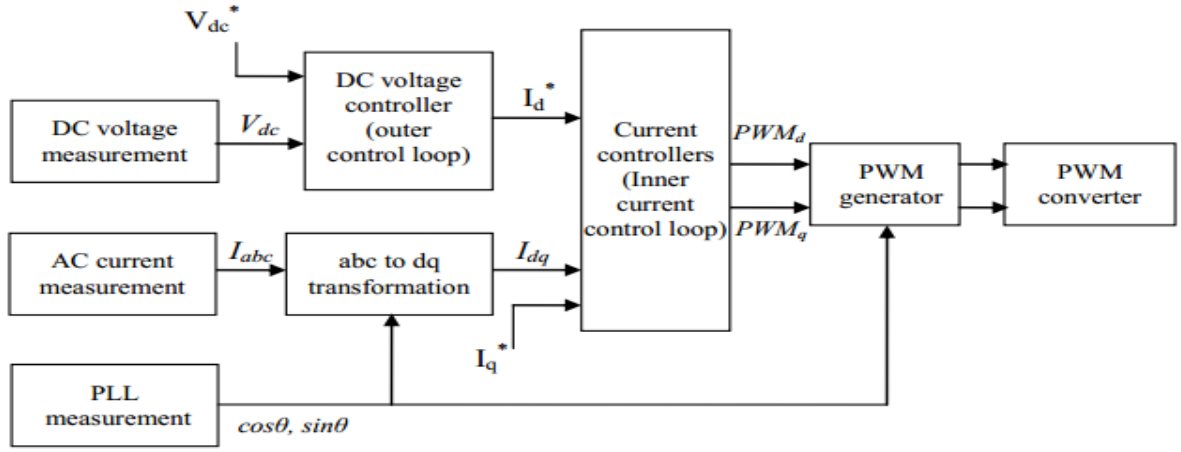

Figure 4.2: Vector control strategy [30].

The vector control strategy comprises the transformation of the three phase quantities to the dq synchronous reference frame. By using the dq synchronous reference frame, it is possible to control active and reactive power. According to the vector control system, initially three-phase system voltages and currents are referred as vectors in a stationary $\alpha\beta$ reference frame and they are transformed into the dq coordinate system [30]. Figure 4.2 shows the vector control methodology which is typically composed of fast inner current control loop and moreover, the

vector controller is completed by additional outer controllers which supply the references for the inner loop [24], [46].

The transformation into dq coordinates is shown as in Eq. (4.1) [30], [46]. Figure 4.3 shows the transformation of the three-phase quantities into the $\alpha\beta$ reference frame utilizing Clark transformation [30] by using Eq. (4.1). By utilizing a Park Transformation, $\alpha\beta$ frame to dq transformation can be written as in Eq. (4.2) [30].

$$\begin{bmatrix} X_\alpha \\ X_\beta \end{bmatrix} = \frac{2}{3}\begin{bmatrix} 1 & \cos\gamma & \cos 2\gamma \\ 0 & \sin\gamma & \sin 2\gamma \end{bmatrix}\begin{bmatrix} X_a \\ X_b \\ X_c \end{bmatrix} \quad \text{where} \quad \gamma = 2\pi/3 \tag{4.1}$$

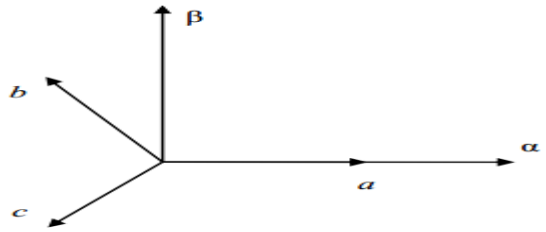

Figure 4.3: Stationary *abc* and $\alpha\beta$ reference frame [30].

$$Xdq = X\alpha\beta.e^{-j\theta} \tag{4.2}$$

The vectors of $X\alpha(t)$ and $X\beta(t)$ rotates with the angular frequency $\omega(t)$ in rad/s. By utilizing the transformation angle θ derived from a phase-locked loop (PLL), the matrix form of Park Transformation is attained as in Eq. (4.3) [30], [46].

$$\begin{bmatrix} X_d(t) \\ X_q(t) \end{bmatrix} = \begin{bmatrix} \cos[\theta(t)] & \sin[\theta(t)] \\ -\sin[\theta(t)] & \cos[\theta(t)] \end{bmatrix}\begin{bmatrix} X_\alpha(t) \\ X_\beta(t) \end{bmatrix} \tag{4.3}$$

Vectors of $Xd(t)$ and $Xq(t)$ represent the currents. $Xd(t)$ provides required power to the DC bus and $Xq(t)$ determine the reactive power condition. The phase angle of the grid voltage $\theta(t)$

provides the decoupling of components for independent control of power. The angle $\theta(t)$ is given as in Eq. (4.4) [30].

$$\theta = \tan^{-1}\left(\frac{v\beta}{v\alpha}\right) \tag{4.4}$$

Where $v\alpha$ and $v\beta$ are the components of voltage in $\alpha\beta$ reference frame [30]. The fundamental current and voltage components become dc variables and therefore in order to reduce steady-state errors, PI controllers are required [30]. The components of the reference voltage from the PI controller are transformed back to three phase values and utilized as inputs to the PWM.

4.2 Control Strategy for the Farm Side Voltage Source Converter

The main purpose of the vector control strategy of the farm side VSC is to control the AC voltage. In this control scheme, two control loops are used in order to control the AC side voltage, including inner control loop which controls the farm side current and outer control loop which controls the voltage drop on the AC side filter capacitance [48].

The farm side converter is utilized to interface between DC-link voltage and the load. The farm side VSC control provides the regulation of the frequency and voltage at the customer load. Figure 4.4 shows the farm side voltage source inverter control strategy. The currents Ia, Ib, Ic and the voltages Va, Vb, Vc are measured and transformed from abc reference frame to dq reference frame utilizing chosen load voltage frequency. The equations of voltage by utilizing dq transformation in the rotating reference frame are given in Eq. (4.5) [49].

$$Vd = Vd_i - L\frac{di_d}{dt} + \omega.L.iq \quad , \quad Vq = Vq_i - L\frac{di_q}{dt} - \omega.L.id \tag{4.5}$$

Hence, the active and reactive power can be calculated by using Eq. (4.6).

$$P = \frac{3}{2}(Vd.\mathrm{id} + \mathrm{Vq}.\mathrm{iq}) \quad , \quad \mathrm{Q} = \frac{3}{2}(Vd.\mathrm{iq} + \mathrm{Vq}.\mathrm{id}) \tag{4.6}$$

Where $Vq = 0$ and $Vd = [V]$, and the equations of power are given as in Eq. (4.7):

$$P = \frac{3}{2}(Vd.id) = \frac{3}{2}[V].id \quad , \quad Q = \frac{3}{2}(Vd.iq) = \frac{3}{2}[V].iq \tag{4.7}$$

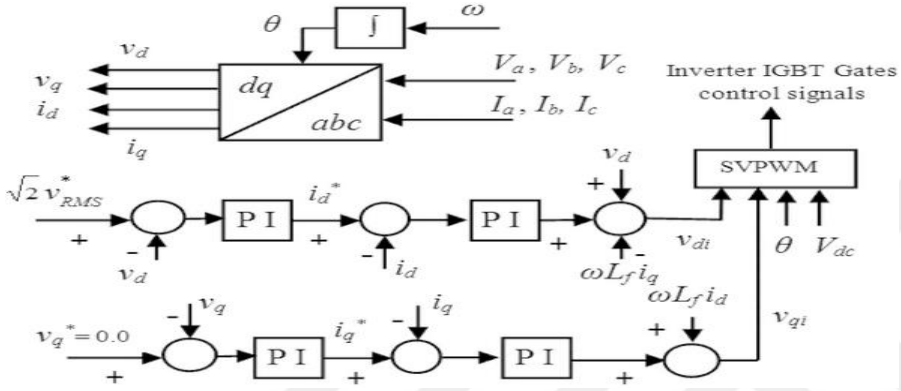

Figure 4.4: The farm side voltage source converter control strategy [49].

Hence, the active and reactive power are controlled by controlling the components of direct and quadrature, respectively. In addition, demand voltage can be given in Eq. (4.8). Where $Vrms^*$ is the RMS reference value of the output voltage. PI controllers are utilized to regulate the currents of output load in inner control loops and to regulate the voltages of output load in the outer loops [49].

$$Vd^* = \sqrt{2} \times Vrms^* \tag{4.8}$$

4.2.1 Inner Control Loop Design

Figure 4.5 shows the structure of the inner current control loop in the synchronous frame. In this design, the plant for d and q current loop is represented as $\frac{1}{sL}$, L is referred as the filter inductance value. . According to [47], the control of inner current loop has to be fast in order to make sure the converter operates at the correct current demand.

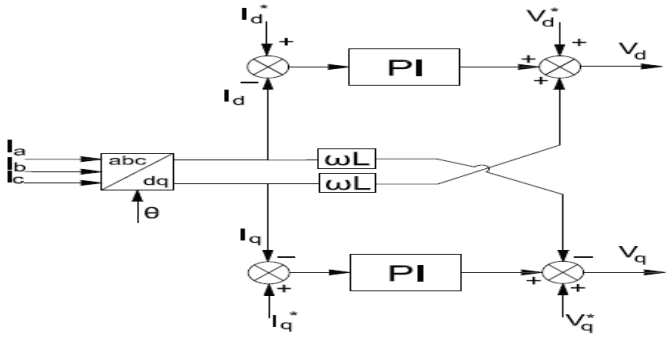

Figure 4.5: The overall structure of the inner current controller in the synchronous reference frame [50].

4.2.2 The AC Voltage Controller Loop

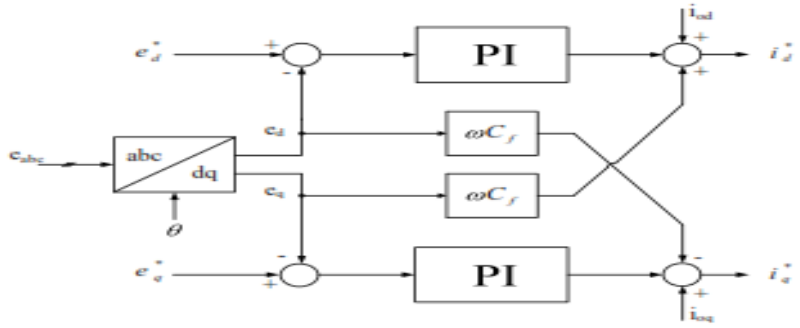

Figure 4.6: The AC voltage controller structure in the synchronous reference frame.

After achieving the proper inner current control loop design, the AC voltage can be controlled with their corresponding references. Figure 4.6 shows the structure of the AC voltage controller loop in the synchronous frame. In this design, the plant for d and q current loop is represented as $\frac{1}{sC}$, C is referred as the filter capacitance value.

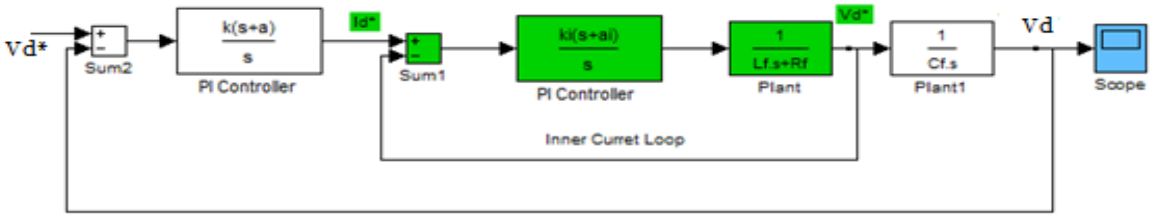

Figure 4.7: AC Voltage Control Loop block diagram.

Figure 4.7 illustrates the cascade control schema, including inner and outer control loop which acts the whole AC voltage control. In this design, the outer control loop bandwidth is chosen 10 times slower than those of the inner loop and therefore, the outer control loop bandwidth and the damping factor are chosen as $\omega_n = 20\,\text{Hz}$ and $\xi = 0.8$, respectively. The detailed calculation of the PI controller for the AC Voltage controller loop is shown in Appendix D. Therefore, the PI controller is obtained as $\frac{k(s+a)}{s} = \frac{0.02(s+78.8)}{s}$.

4.3 The Grid Side Control Design

The aim of the grid side vector control strategy is to keep the DC side voltage constant, whereas controlling the reactive power flow through the grid. The grid side control strategy consists of two control loops, including fast inner control loop which controls the grid current, and an external voltage loop (outer control loop) which controls the DC side voltage.

The inner current control loop plays a significant role in the issues of power quality like low THD rate and good power factor while the voltage control loop provides power flow balance in the system. The synchronous reference frame control utilizes a reference frame transformation abc to dq which transforms the grid current and voltages into dq frame [51]. The voltage transformed detects frequency and phase of the grid, whereas current transformed controls the grid current. Therefore, the control variables are obtained as DC values, thus controlling and filtering becomes easier [51]. The schematic of the grid side VSC control structure is shown in Figure 4.8. The DC side voltage is fed from the wind farm model. The reference for active current control is set by the DC side voltage whereas the control reference of reactive power is set to zero. It can be concluded that the control of reactive power is not applied here. **Phase Lock Loop (PLL):** Grid synchronizations have a major importance for the grid connected systems and it provides synchronizations for the output frequency and grid voltage phase with grid current utilizing

different transformation. Figure 4.9 demonstrates the used method for the derivation of the phase angle θ required for the transformation of $abc-dq$ and $dq-abc$ in control loops.

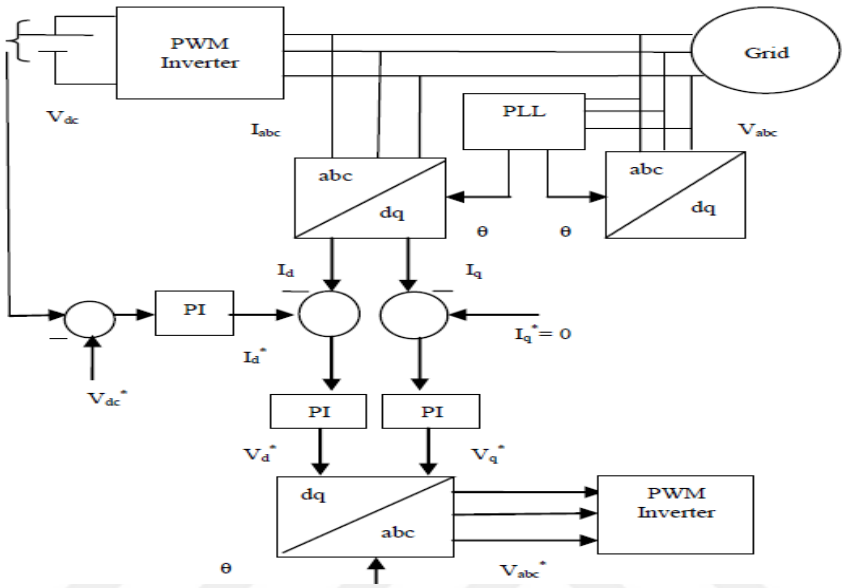

Figure 4.8: The general structure for the d-q reference frame control [51].

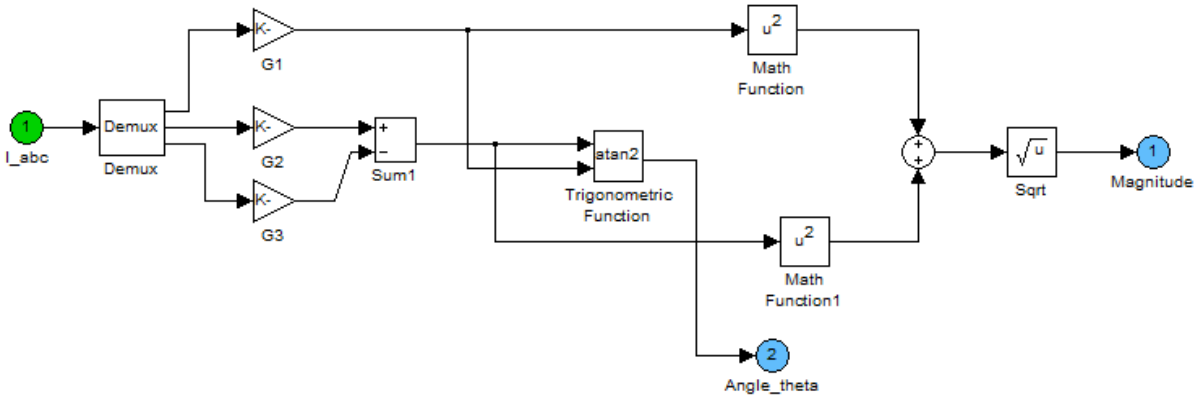

Figure 4.9: The structure of the phase angle θ derivation for the transformation.

Figure 4.10 demonstrates the current transformation performance for the design in Figure 4.10. The waveforms obtained from Figure 4.10 shows the expected dq axis current magnitude and the phase angle θ which is required for the transformation of abc to dq reference frame and vice versa for the defined control loops. The angle θ is calculated by using the "arctan" trigonometric function utilizing the corresponding reference point for the transformation. Figure 4.11 shows the transformation of abc coordinates to dq axis frame by using the extraction of phase angle as

described in Figure 4.10. This transformation concept is used in all Simulink models existing in this thesis.

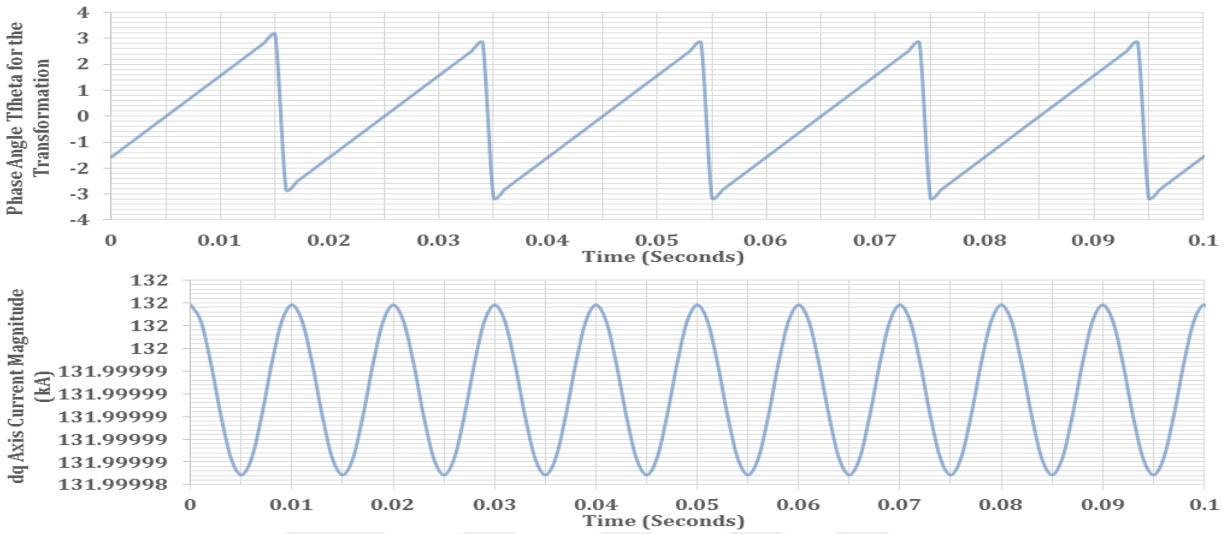

Figure 4.10: The simulation results of the phase angle and magnitude in GS-VSC design.

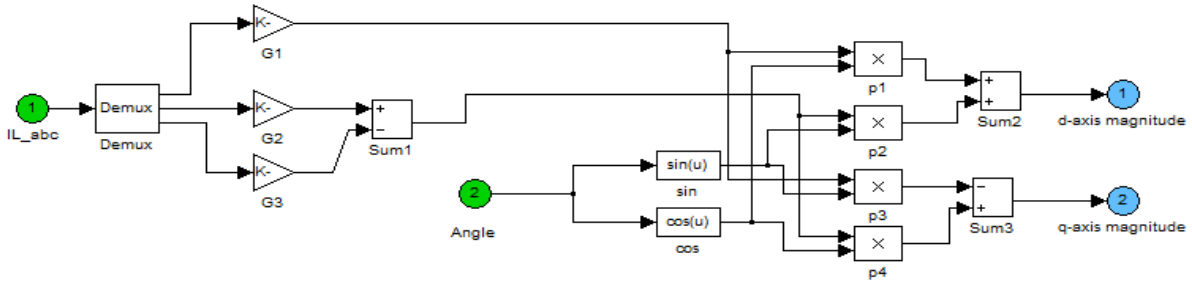

Figure 4.11: The transformation of ABC coordinates to dq axis reference frame.

4.3.1 Design of both outer control loop and inner control loop

Figure 4.12 shows the cascade control scheme, including an inner current control loop and outer DC link voltage control loop. **Inner Control Loop Design:** Grid side voltage orientation plays an important role for enabling a platform for the control of active power as independent from the reactive power flow between the grid side converter and the AC grid.

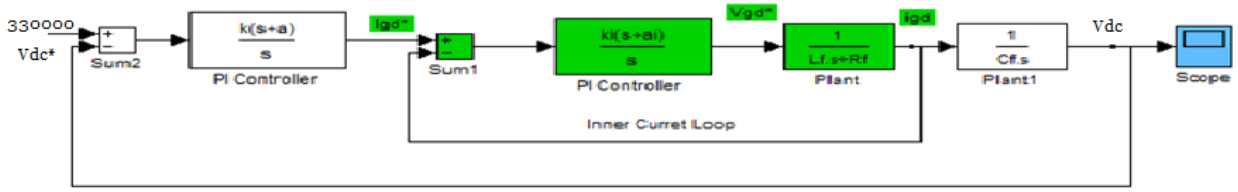

Figure 4.12: The cascade control scheme of the GS-VSC.

This is achieved by controlling the components of the grid current. Hence PI controller is used for the regulation of the components of the current *Igd* and *Igq* by utilizing the reference components of the voltage *Vgd** and *Vgq**. In this control design, the closed loop bandwidth and damping factor are chosen as $\omega_n = 200$ Hz and $\xi = 0.8$, respectively. The values of the grid side inductance is $L = 0.001$ H. The detailed calculation of the PI controller for the inner loop is given in Appendix F. The obtained PI controller is $\frac{k(s+a)}{s} = \frac{2(s+785.6)}{s}$.

Outer Control Loop Design: As seen in Figure 4.12, the outer DC control loop utilizes the *d* axis current *Igd* for the regulation of the DC side voltage**.** The design of PI controller is the same as inner control with 20 Hz bandwidth and a 0.8 damping factor. By using the DC link capacitance value is $C = 0.1$ F , the detailed calculation of the PI controller for the outer control loop is given in Appendix F. The obtained PI controller is $\frac{k(s+a)}{s} = \frac{20(s+79)}{s}$.

CHAPTER 5: SIMULATION AND ANALYSIS

5.1 Matlab Simulink Model - 1

Objective: To construct an average value non-switching model with proper control and illustrate its operation of the farm side voltage sourced converter (FS-VSC). It is shown that the FS-VSC can control the AC voltage as independent from the DC load size and the current source amplitude. The Simulink model is constructed by assuming that the VSC can fully control its AC

side voltage and therefore, there is no power loss in the converter, so the input AC power equals the output DC power.

Configuration Parameters used in Matlab/Simulink:

Type: Variable-Step; Solver: ODE45; Max Step Size: 0.0001 and Min Step Size: 0.000001 Relative Tolerance: 0.001; Absolute Tolerance: Auto.

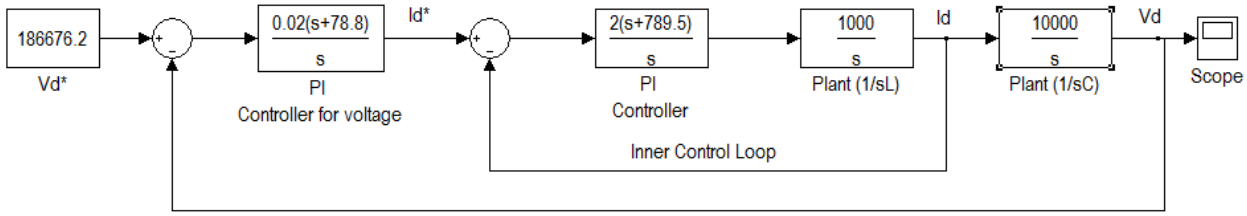

Figure 5.1: The implementation of the AC voltage controller loop for FS-VSC in Matlab/Simulink.

Parameters used in the simulation: The calculation of parameters used in the simulation is shown in Appendix C. AC current source amplitude = $252.5\ \text{A}$; Frequency= $50\ \text{Hz}$. AC Filter Values: Inductance $L = 1\ \text{mH}$, DC side capacitance value = $0.1\ \text{F}$ and DC Voltage = $330\ \text{kV}$, DC Link Load = $1200\ \Omega$.

Simulink Model: The model seen in Figure 5.1 illustrates the operation of the farm side voltage source converter (FS-VSC) utilizing the non-switching model with a proper control in order to obtain the AC voltage controlled by the FS-VSC as independent from the DC load size and the current source amplitude. Figure 5.2 demonstrates the average value model of the VSC with subsystem for Farm Side, which consists of its control system and current source.

Simulink Diagram for Control Structure: Figure 5.3 illustrates the implemented control structure of the farm side voltage source converter (FS-VSC) to control the AC Side Voltage as independent from the DC load size and the current source. The calculations of the PI controller for

voltage control loop and inner control loop are shown in Appendix D. PI Controller (Voltage Control Loop) is $\frac{0.02(s+78.8)}{s}$ and PI Controller (Inner Control Loop) is $\frac{2(s+789.5)}{s}$.

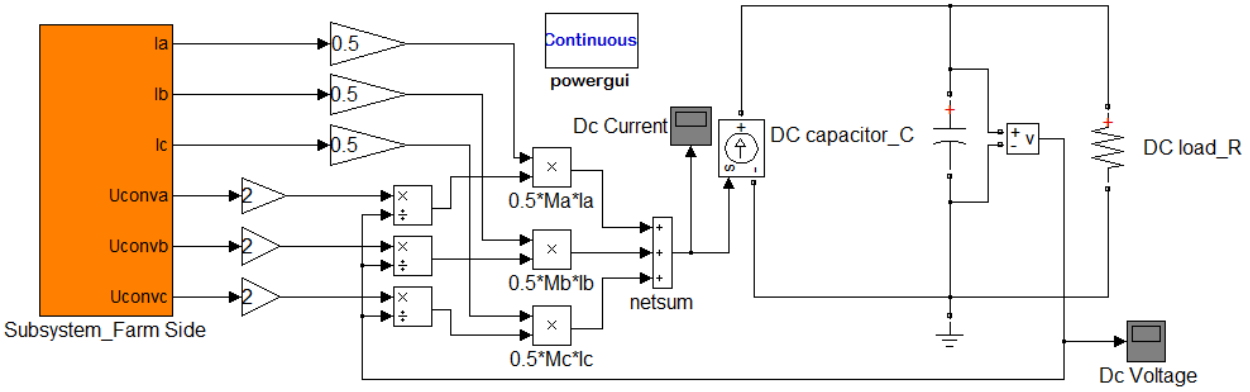

Figure 5.2: Simulink diagram of the structure of the Farm Side VSC.

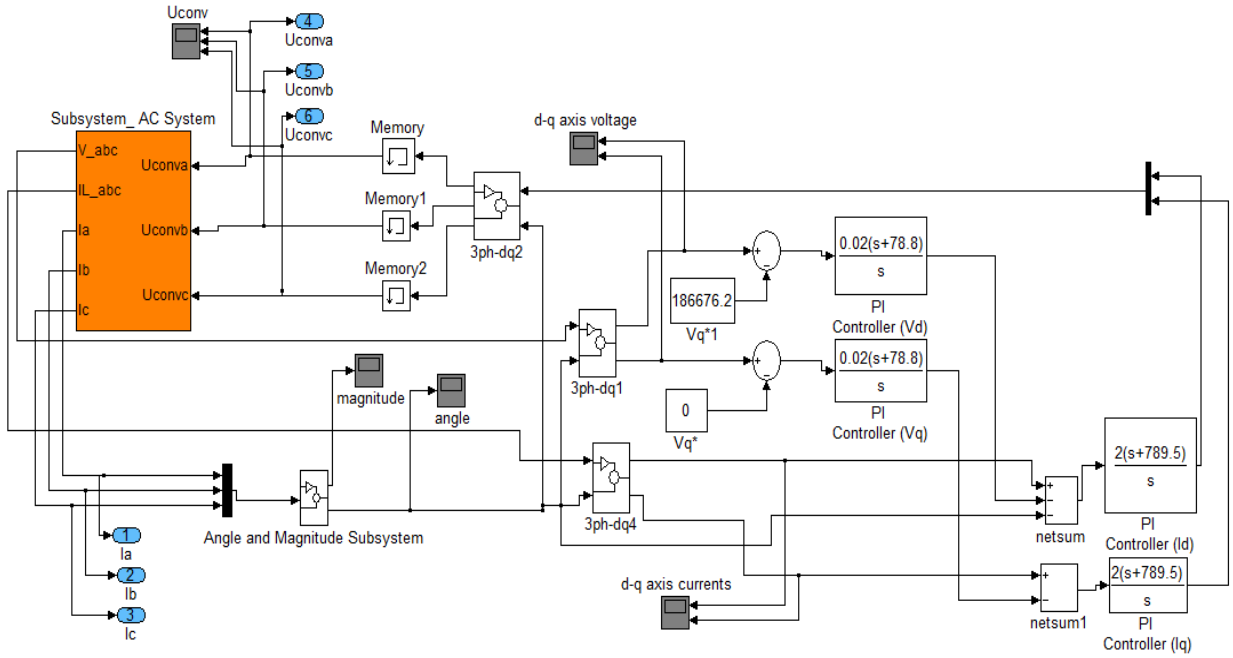

Figure 5.3: The Simulink diagram of the Farm Side Converter control.

Subsystem for Constant Input Source: Figure 5.4 shows the AC current used as a constant source for the farm side voltage source converter (FS-VSC) operation. According to this model, the amplitude of the AC Current Source used is $252.5\,A$ and its calculation is shown in Appendix C.

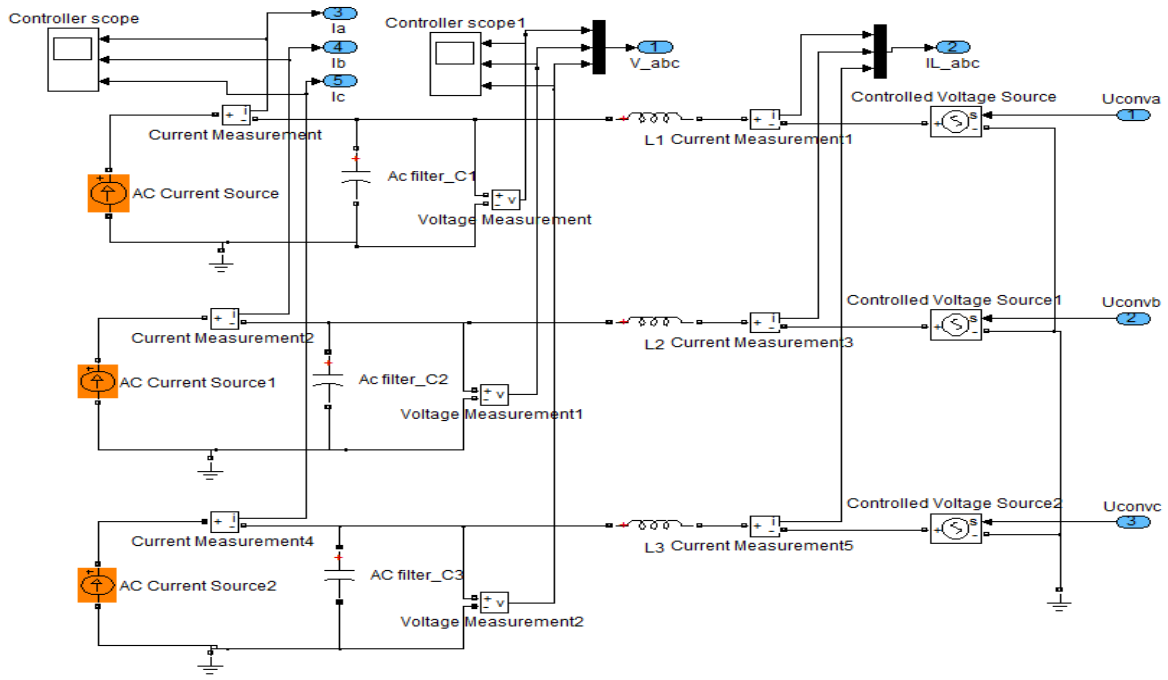

Figure 5.4: Simulink model for the Constant Input Source in the Farm Side.

5.2 Simulation Results of Simulink Model - 1:

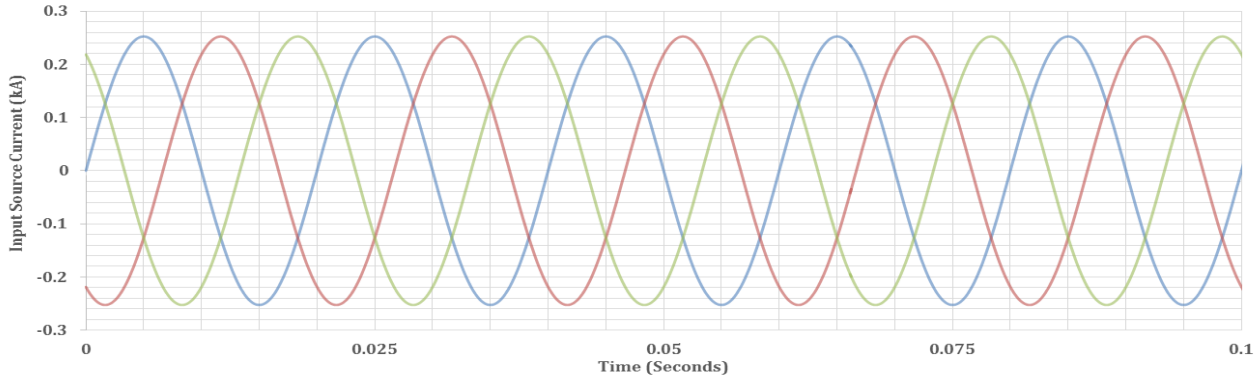

Figure 5.5: The waveforms of the input current source for the Farm Side VSC.

Comment for Input current source: Figure 5.5 demonstrates a constant current source waveform which has 252.5 A magnitude applied on the system for the FS-VSC operation. The calculation of the current source magnitude is given in Appendix C.

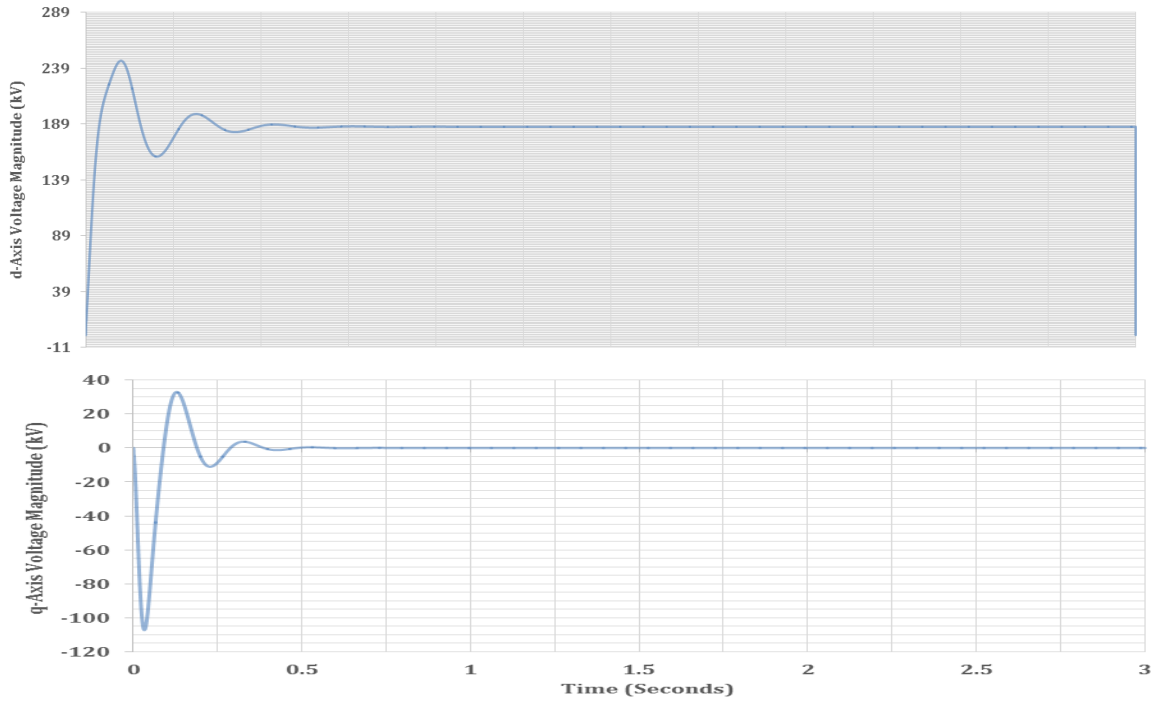

Figure 5.6: The AC voltage controller loop performance in the Farm Side.

Comment for dq axis voltage: The waveforms shown in Figure 5.6 demonstrates the AC voltage control loop performance and this has an outer voltage control loop and an inner current control loop with a reference voltage of 186676V. It is clear that d and q axis voltage is able to reach fast to its reference voltage. The d axis voltage (Vd) provides the required power flow for the DC link and q axis voltage (Vq) attains the reactive power condition. It is observed from Figure 5.6, q axis voltage equals to zero, this means that there is no reactive power condition here.

Comment for AC Voltage: The graphs as seen in Figure 5.7 illustrate the AC side voltages on the AC filter capacitance and on setting a reference voltage for the AC voltage controller loop. It is observed that there is a significant change in voltage at the time of 0-0.3 second. However, this voltage is able to be maintained to a controllable level by the FS-VSC as independent from DC load size and input source.

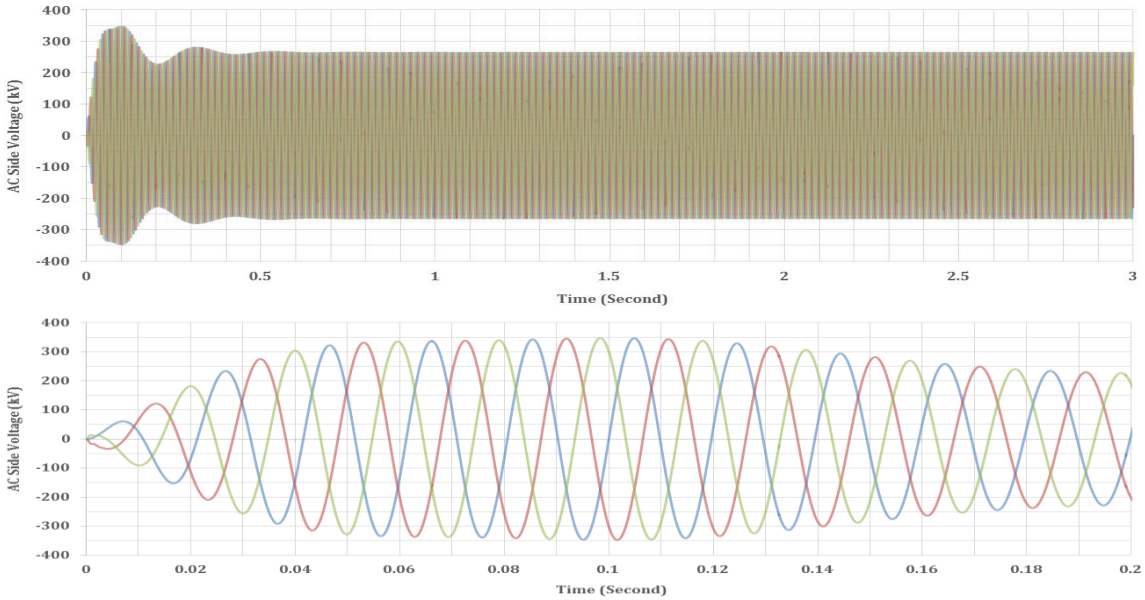

Figure 5.7: The waveforms of the controlled AC voltages in the Farm side by the FS-VSC; a) 0 - 3 s, b) 0 - 0.2 s.

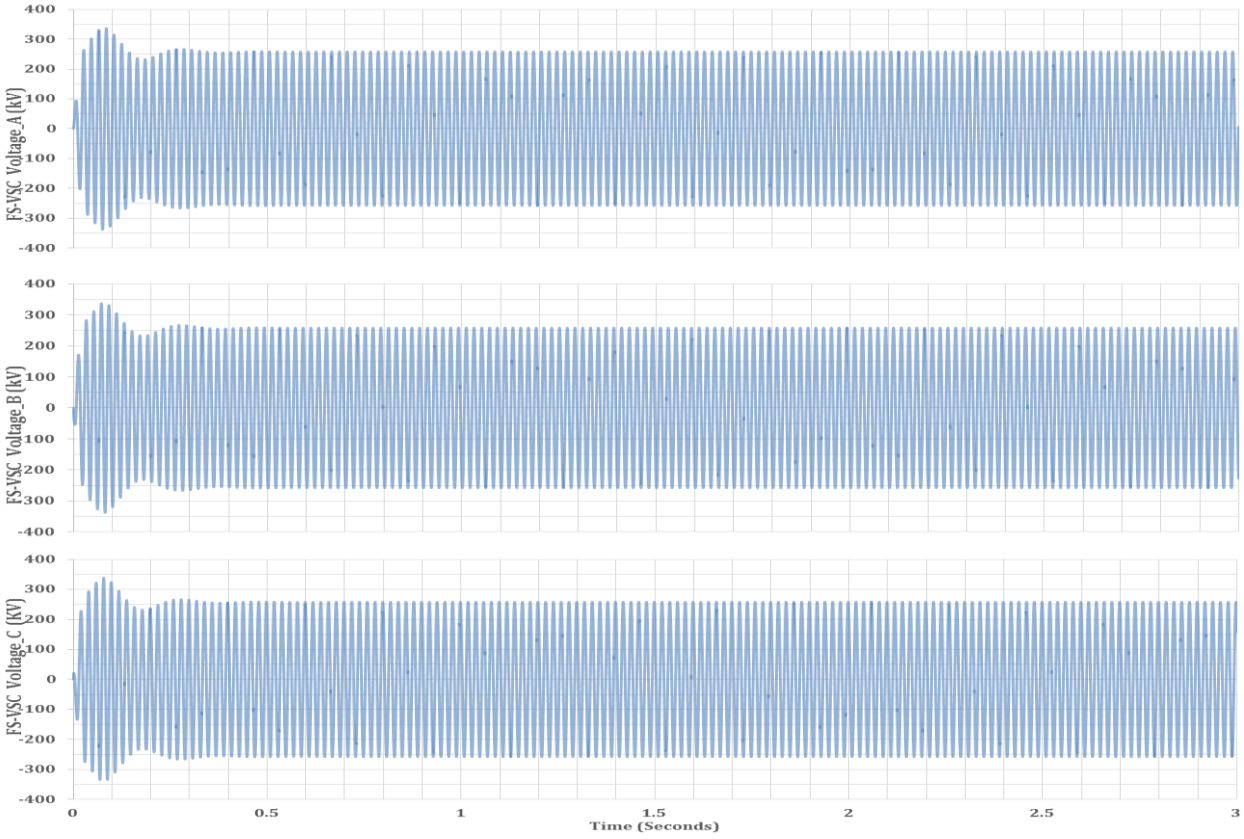

Figure 5.8: Each phase of voltage waveform across the FS-VSC.

Comment for FS-VSC Voltage: The graphs as seen in Figure 5.8 illustrate that the AC voltage can be controlled by FS-VSC as independent from the current source amplitude $252.5\ \text{A}$ and the DC load resistance of $1200\ \Omega$ and the DC side capacitance of $0.1\ \text{F}$.

Comment for Dc link voltage and current: The waveforms as seen in Figure 5.9 demonstrates the expected current and voltage across the DC side capacitance $(0.1\ \text{F})$, respectively; on implementing the current source amplitude of $252.5\ \text{A}$ and a DC side load resistance of $1200\ \Omega$. It is clear that a stable DC link output is obtained, but needs a voltage controller so as to keep its voltage constant.

Case 2: Subsystem of the Simulink Diagram: The Simulink model as seen in Figure 5.10 shows the AC current source with step changes for the FS-VSC operation and therefore the AC voltage is controlled in all cases by the converter. It is also demonstrated that the variations of the DC voltage with current source and the changes of the load during the FS-VSC operation in controlling AC voltage.

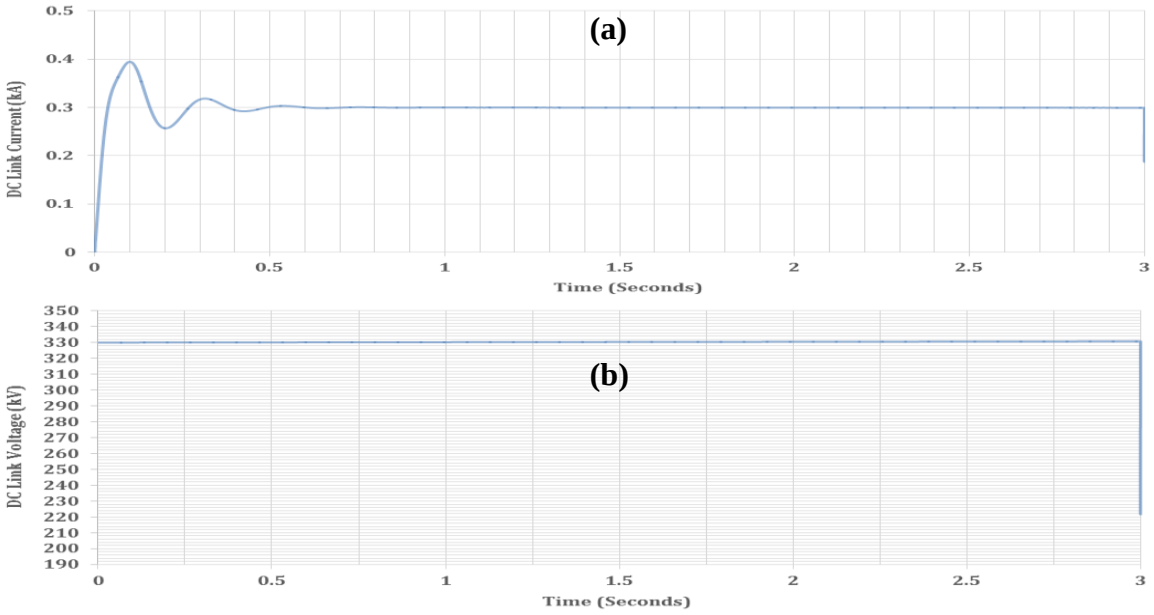

Figure 5.9: The waveform of the current (a) and voltage (b) across the DC side capacitor.

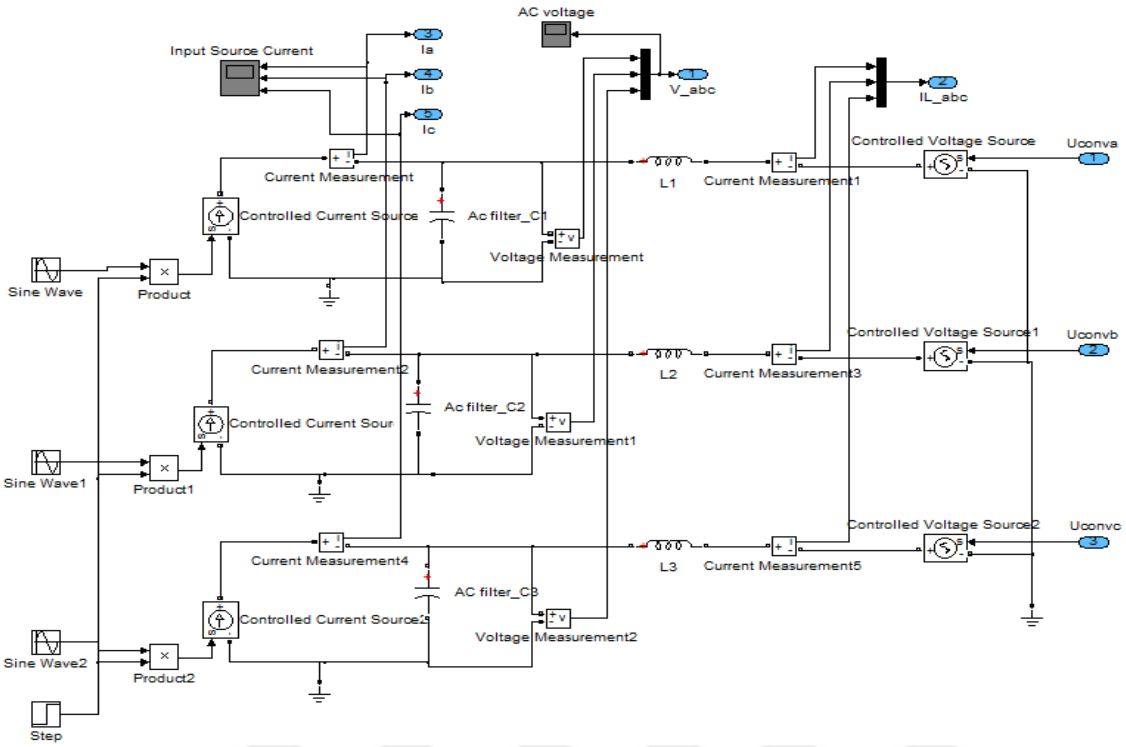

Figure 5.10: Simulink model for a varying Input source on the Farm Side.

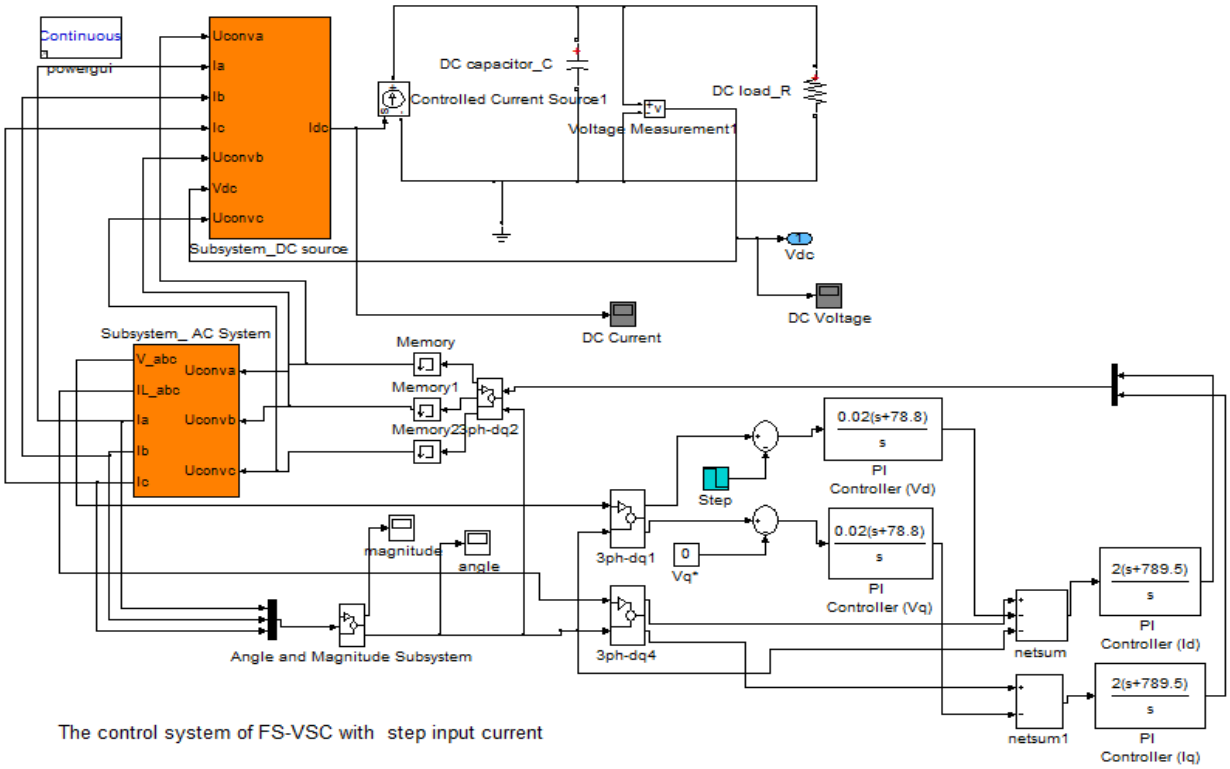

Figure 5.11: The control system model of FSC-VSC with step input current.

The control system model of FS-VSC with a step input current source is shown in Figure 5.11, the d axis voltage component demand is referred as Vd^* .According to Figure 5.11, Vd^* is shown as the step input, which have $220\,\text{kV}$ of initial value and $132\,\text{kV}$ of final value. The q axis voltage demand component is $Vq^* = 0$.

Parameters used in the model: AC current source: Sinusoidal wave with the $1amp$ amplitude; frequency $= 50\,\text{Hz}$; Step input on implementing a load as initial value of $151.5\,\text{A}$ and stepped to $252.5\,\text{A}$ at the step time of 2 seconds. Filter used at the Farm Side: AC capacitance$= 0.1\,\text{mF}$; AC inductance = 1 mH.

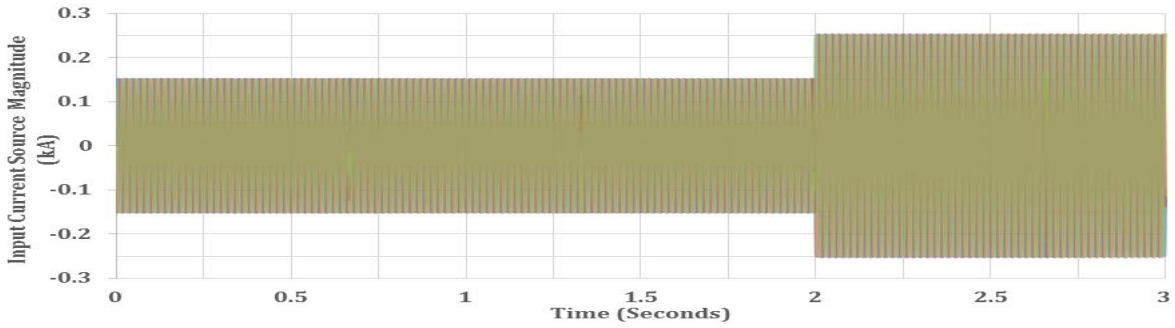

Figure 5.12: The waveform the input current source as Step Response in the Farm Side.

Comment for Input Current Source: Figure 5.12 shows the input source current waveform imposed for the Simulink model by implementing a step input, which applies $151.5\,\text{A}$ initial load and then this is stepped to $252.5\,\text{A}$ in a time of 2 seconds; and applying a sinusoidal wave form of the $1\,\text{A}$ magnitude.

Comment for AC voltages: The waveforms seen in Figure 5.13 shows the AC voltage variations across the AC filter capacitor on implementing the current source amplitude of $1A$ with $252.5\,\text{A}$ of a step input value at the time of 2 seconds and on implementing a reference voltage for the AC voltage controller loop at the time of 1 second.

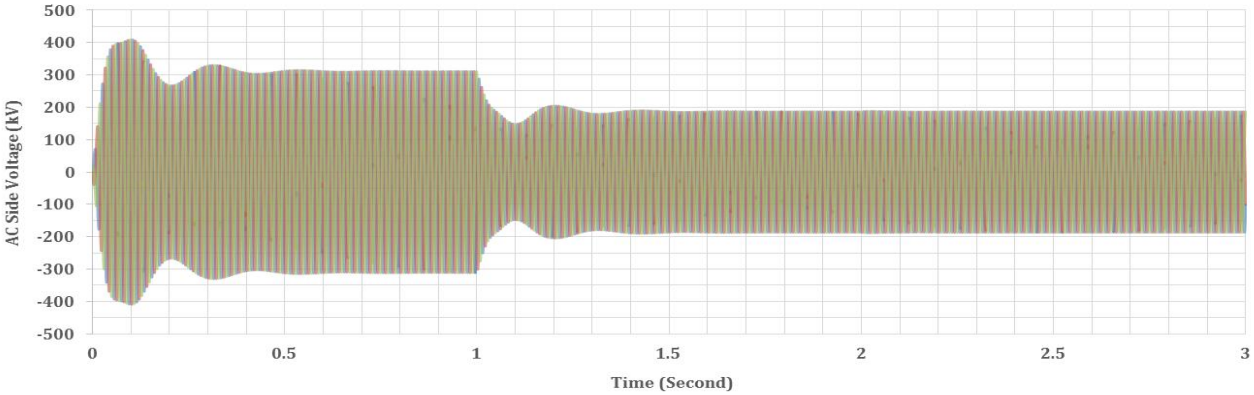

Figure 5.13: The controlled AC Voltages waveform by the FS-VSC.

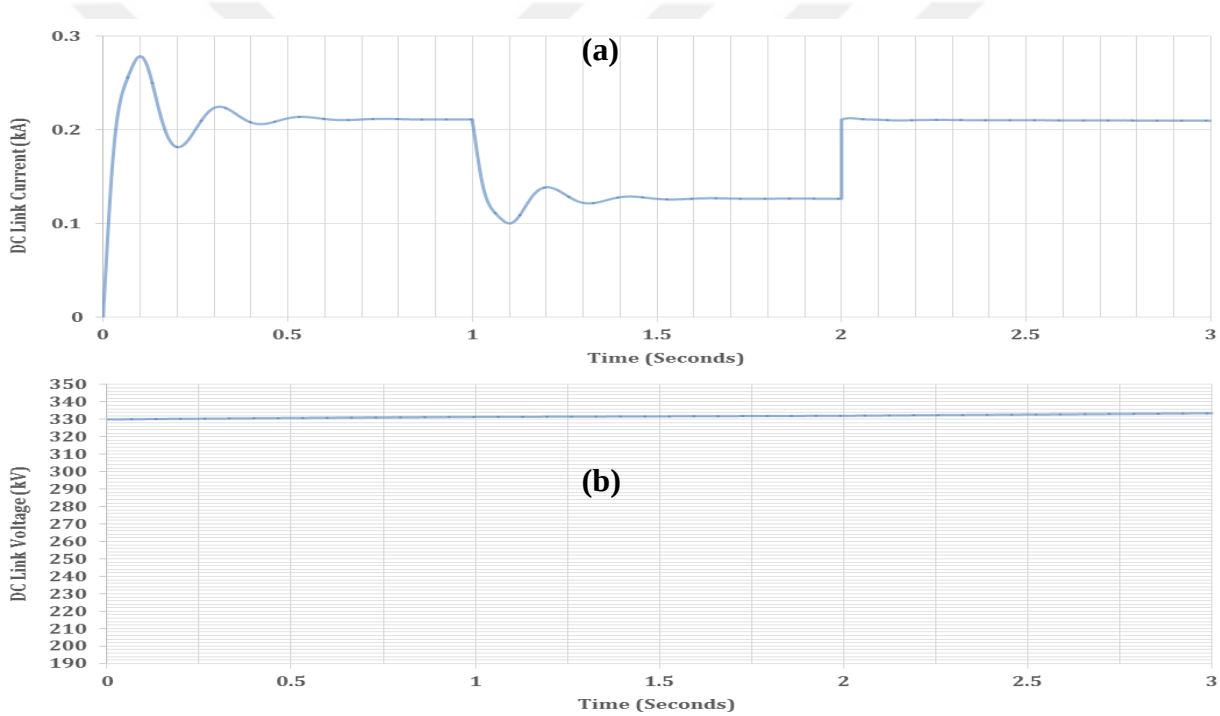

Figure 5.14: The waveform of the DC link current (a) and voltage (b) (with step response).

Comment for DC link current and voltage: The waveforms as seen in Figure 5.14 demonstrates the current and voltage variations in the DC side with load changes and the current source, respectively. It is observed that there are some changes in the DC side due to the step input at a time of 2 seconds and on having a reference (demand) voltage at the time of 1 second. According to the simulation result in Figure 5.14a, the DC link current has many changes based on the DC

load size, therefore a DC voltage controller is required to be able to obtain its value to a controlled state.

5.3 Matlab Simulink Model-2

Objective: To construct an average value non-switching phasor model with proper control and illustrate its operation of the Grid side voltage source converter (GSC-VSC). It is shown that DC voltage can be controlled by the GS-VSC independently of the current source amplitude and DC load size.

Configuration Parameters used in Matlab/Simulink:

Type: Variable Step; Solver: ODE45; Max Step Size: 0.0001 and Min Step Size: 0.000001. Relative Tolerance: 0.001; Absolute Tolerance: Auto

The structure of Control Design

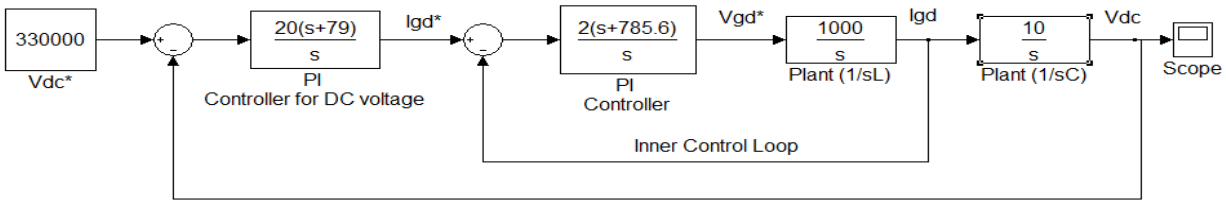

Figure 5.15: The structure of the DC voltage controller loop for GS-VSC in Matlab/Simulink.

Simulink Diagram: Figure 5.16 shows the overall construction a non-switching phasor model with proper control and its operation of the grid side voltage source converter (GS-VSC) in Matlab/Simulink. According to this model, the GS-VSC can control DC link voltage as independent from the current source amplitude and the size of DC load. A controlled DC current source utilized as an input for the controller loop of the DC-link feeds the AC Network over the GS-VSC.

Parameters used in the simulation: The calculation of parameters used in the simulation is shown in Appendix E. Grid Voltage $=132\,\text{kV}$; Peak grid voltage= $132000\times\sqrt{2}=186676.2\,\text{V}$ seen in Appendix E . Grid side impedance values: Inductance $L=1\,\text{mH}$; Frequency$=50\,\text{Hz}$; DC load value is $100\,\Omega$. DC side capacitance = $0.1\,\text{F}$ and DC Voltage = $330\,\text{kV}$. The calculation of DC link capacitance and DC voltage is given in Appendix E.

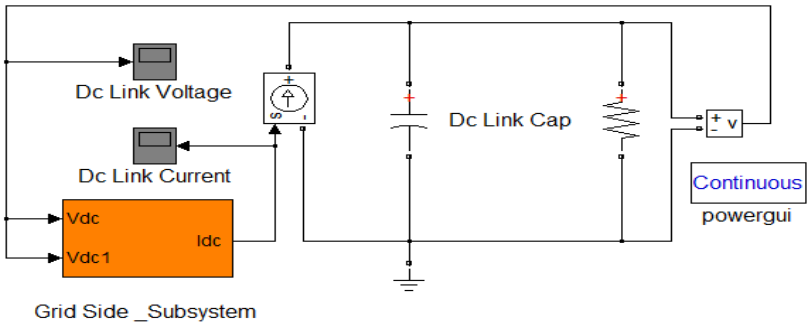

Figure 5.16: The demonstration of the Grid Side Voltage Source Converter subsystem and its DC link in Simulink.

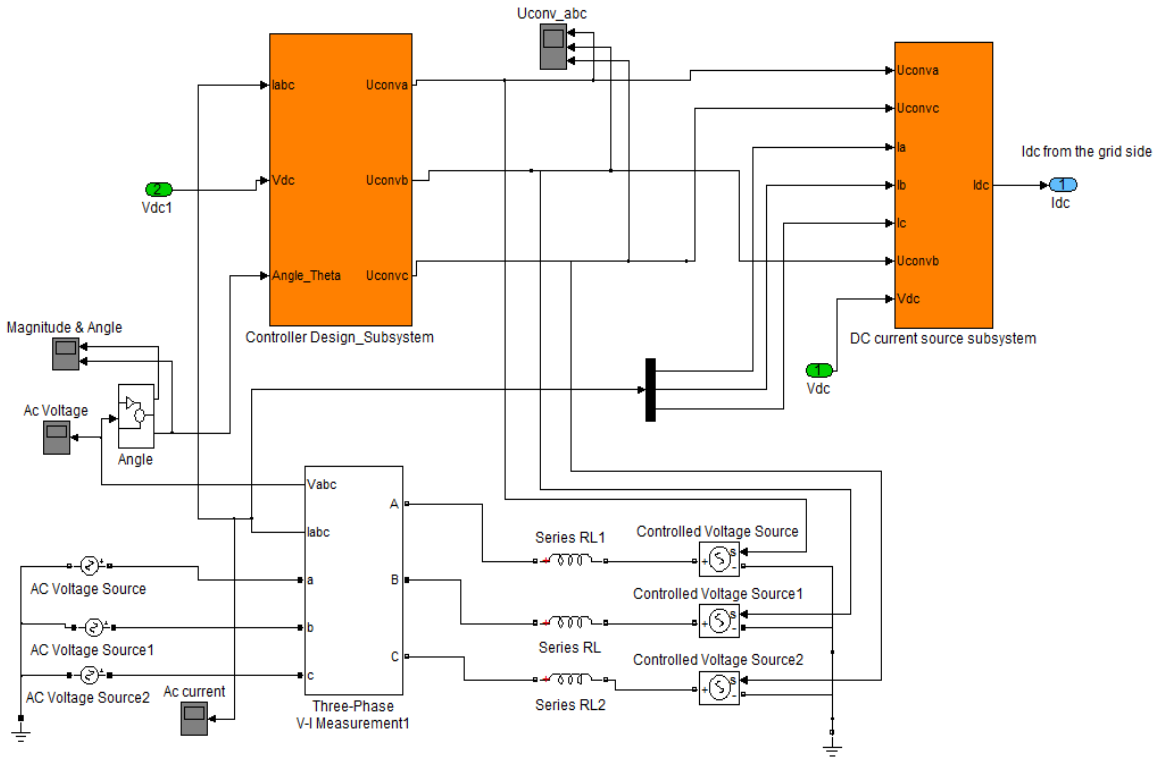

Figure 5.17: The Grid Side VSC Subsystem for the Simulink Diagram.

Grid Side Subsystem of the Simulink Diagram: The Simulink model in Figure 5.17 consists of the AC grid connected with two subsystems, including the Controller Design and DC current source subsystems. The average model of voltage source converter is designed using the AC current for the aim of obtaining the DC current from the AC grid and this model is demonstrated in the DC current source subsystem by assuming that the DC voltage can be fully controlled by the VSC and there is no power loss in the converter, therefore input DC power equals the output AC power.

Used parameters: RMS Grid Voltage= $132\,\text{kV}$ Peak grid voltage $=186.676\,\text{kV}$; Grid side impedance values: Inductance $L=1\,\text{mH}$.

Controller Design Subsystem of the Simulink Diagram: Figure 5.18 demonstrates the structure of the control design for the grid side voltage source converter (GS-VSC) operation in order to obtain DC voltage controlled as independent from the DC load size and the current source. It is clear that the Three-Phase Voltage Current (V-I) Measurement provides reference voltage for the phase angle (θ) calculation which is required for the abc to dq reference frame transformation and also provides the reference current for this transformation. The plant in the control design is AC grid impedance and the controller values are calculated in Appendix F and given as: Inner control loop PI controller: $\frac{2(s+785.6)}{s}$ and Outer (DC Voltage control) loop: $\frac{20(s+79)}{s}$. According to the Figure 5.18, GS-VSC is arranged utilizing the dq axis currents where the DC side voltage is arranged using the d axis current and the regulation of the reactive power can be obtained utilizing the q axis current. The reactive power flow from the grid to the grid side converter is determined by the q axis current demand Iq^*. Figure 5.18 shows Iq^* is set to zero. This means that there is no reactive power flow from the grid side into the grid side converter.

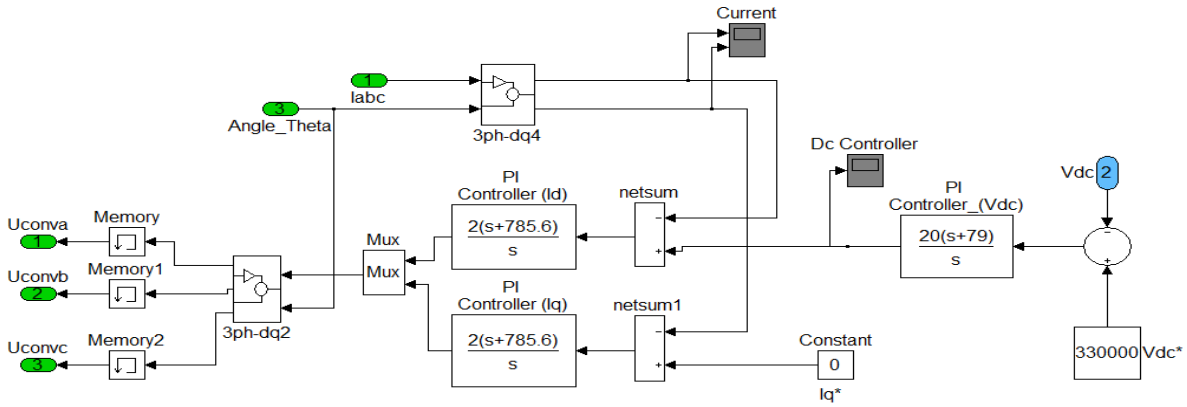

Figure 5.18: The Simulink diagram of the control system design of the grid side voltage source converter.

5.4 Simulation Results of Simulink Model - 2

Comment for DC voltage: Figure 5.19 demonstrates the controlled DC link voltage obtained from the Simulink model. It can be resulted that DC side voltage can be controlled utilizing the grid current. By using the d axis current, the DC side voltage can be regulated. From the Simulink model, the value of the reference DC voltage is $330\,\text{kV}$. It is observed that the DC voltage obtained from the simulation result is able track its reference voltage accurately. The DC voltage becomes stable very fast to its reference voltage. An excellent DC voltage is attained from the simulation.

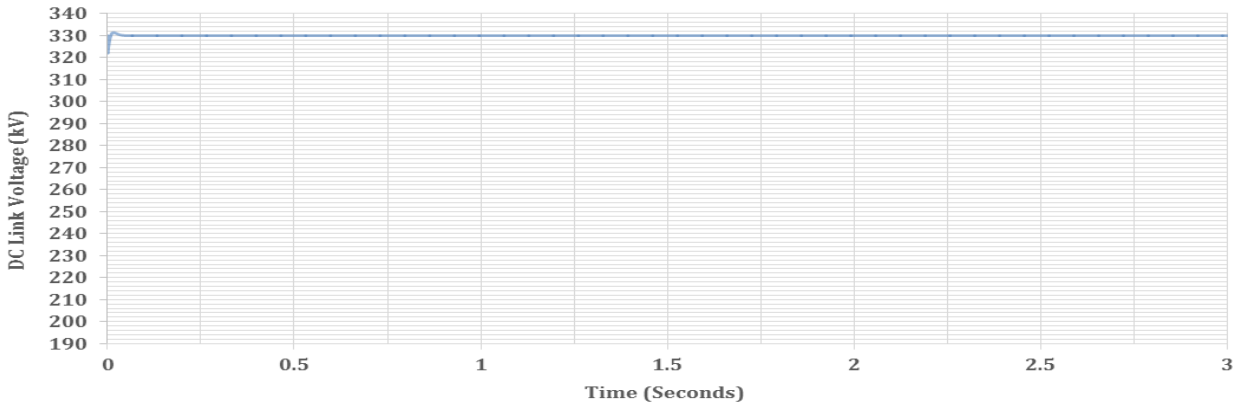

Figure 5.19: The waveform of the controlled DC Link Voltage.

Comment for GS-VSC Voltage: The waveforms of the voltage across the each phase of the GS-VSC are shown in Figure 5.20. According to these graphs, the DC link voltage is maintained at a control state by the grid side converter.

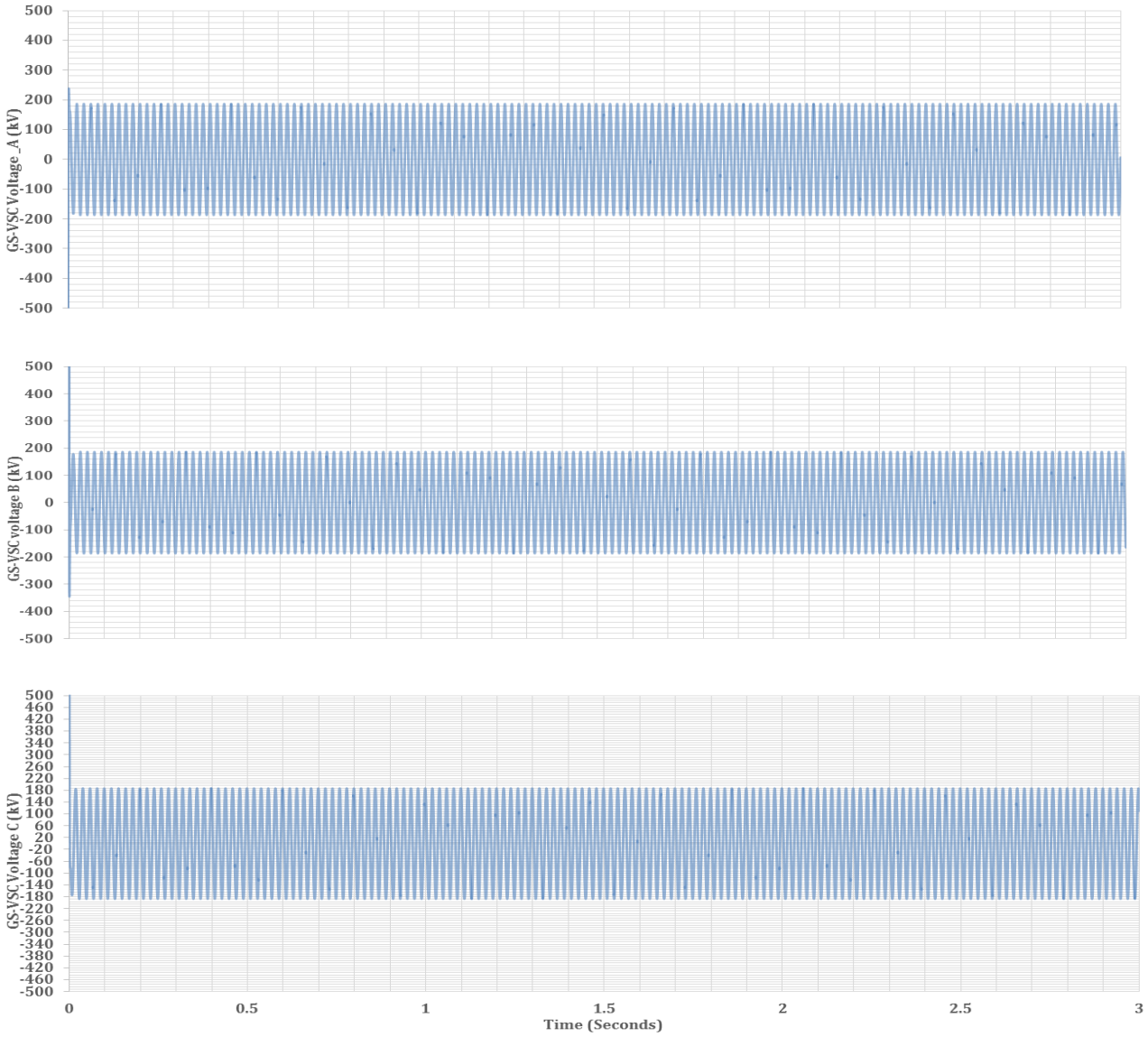

Figure 5.20: The waveforms of the voltages across the each phase of the GS-VSC.

Comment for Grid side current: Figure 5.21 shows the waveforms of the three-phase AC grid currents and through controlling them in the q axis frame. As a result of this, the control of active power flown from the AC grid to the grid side converter is achieved independently of the reactive power by utilizing the grid voltage orientation.

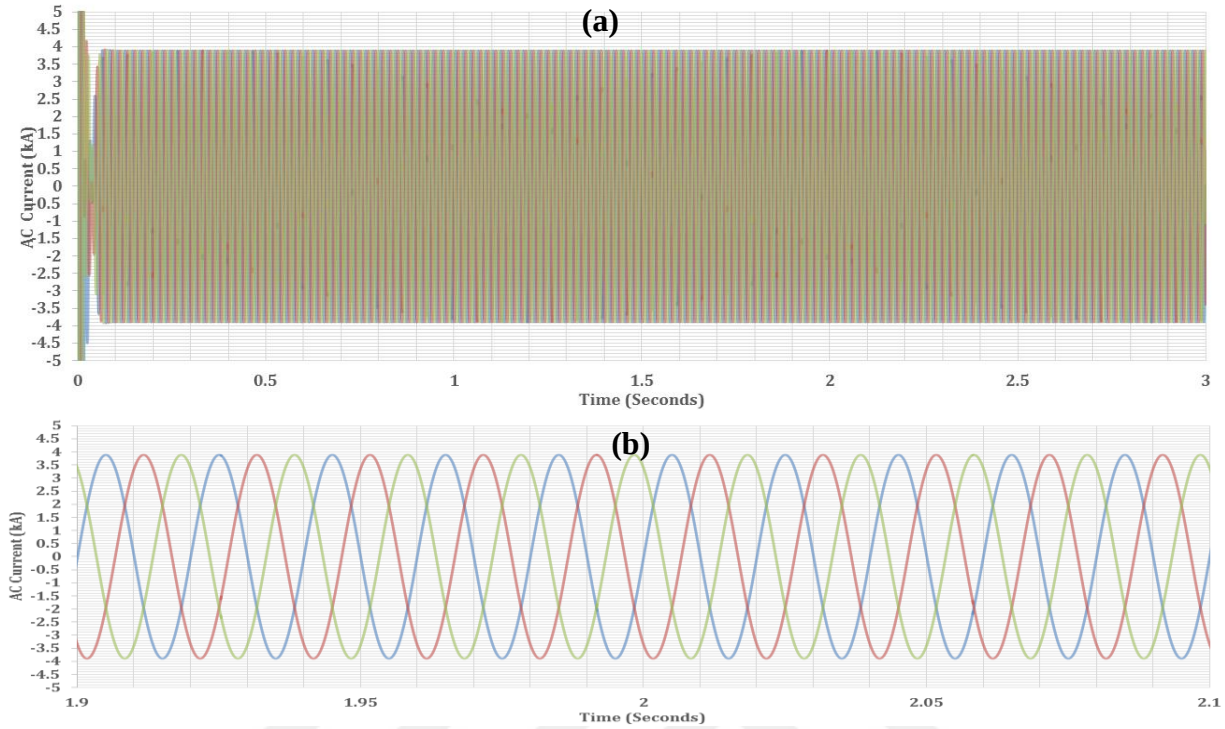

Figure 5.21: The waveforms of the Grid side currents on applying a controlled DC current; a) 0 – 3 s, b) 1.9 – 2.1 s.

Comment for DC Current: Figure 5.22 shows the DC current obtained from the grid side by utilizing the average value model of the VSC in the grid side. The DC current magnitude shows transient until around 0.1 second but it is able to be kept to its expected value fast.

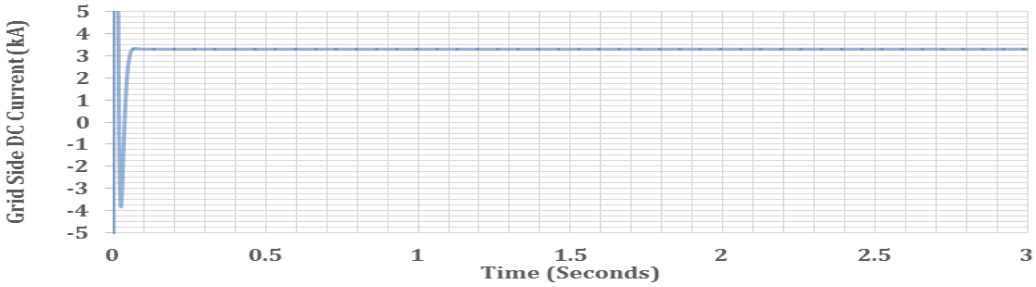

Figure 5.22: The waveform of the DC side current generated from the grid side utilizing the average value model of the VSC.

Comment for DC Voltage: The main objective of the voltage controller is to keep the DC side voltage to a constant value and the control of the power flow through the grid converter. The task of the current regulation and the DC side voltage is achieved by utilizing a PI Controller because it

shows an excellent dynamic and a steady state performance with the grid inverter. The obtained DC link voltage is shown in Figure 5.23.

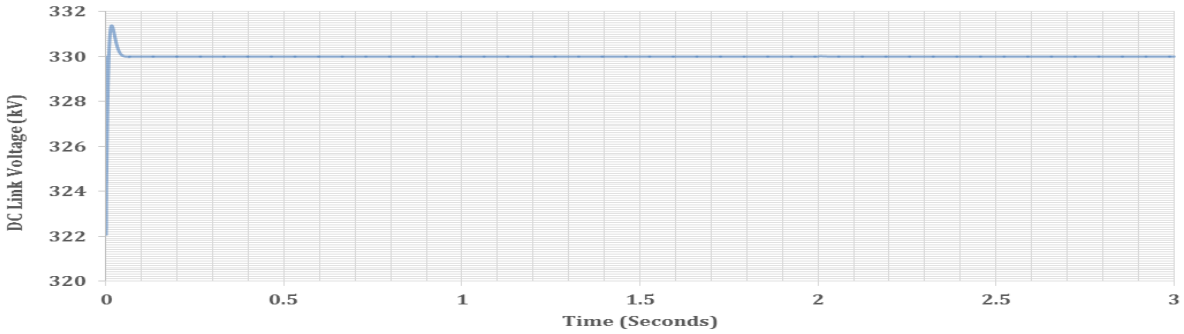

Figure 5.23: The waveform of the obtained DC link voltage utilizing the average value model of the VSC.

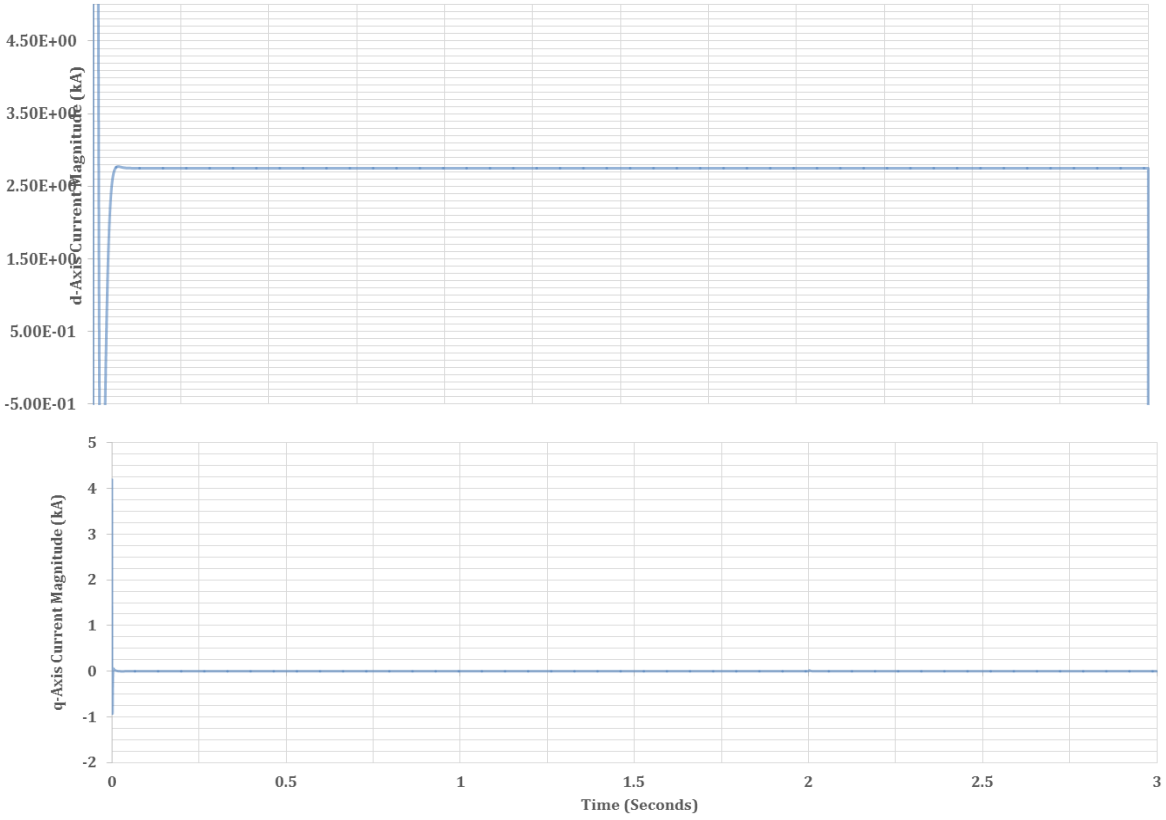

Figure 5.24: The demonstration of the d and q axis current (Input of the inner control loop).

Comment for d-q axis current magnitude: According to Figure 5.24, the transformation of the abc to dq provide Id and Iq dc components. The active current required to maintain the active

power to the grid is controlled by the component of Id . The Iq component value is zero since the reference control is set to zero and the reactive power is not controlled here.

5.5 Matlab Simulink Model - 3

Objective: To construct a completed HVDC link by combining the FS-VSC and GS-VSC and demonstrating its action when it is supplied on the farms side by a constant AC current source.

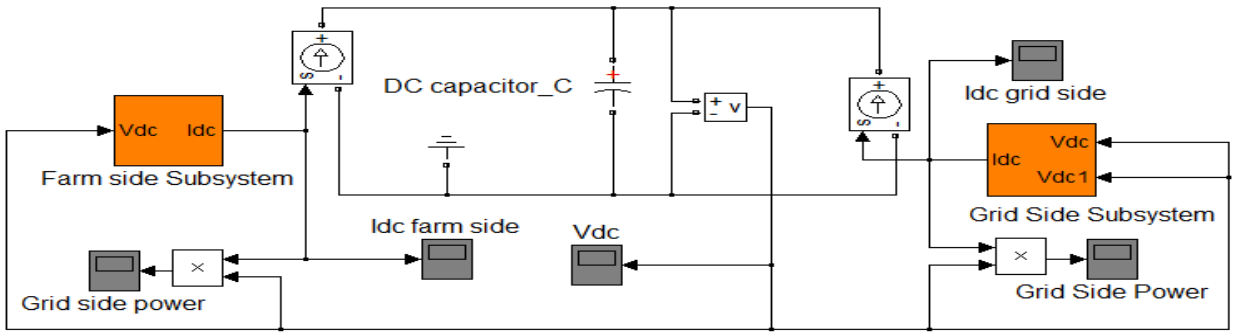

Figure 5.25: The completed HVDC Link by combining the FS-VSC and GS-VSC.

The configuration parameters used in Simulink:

Type: Variable-Step; Solver: ODE45; Max Step Size = 0.0001 s; Min Step Size = 0.000001 s. Relative Tolerance = 0.001; Absolute Tolerance: Auto

Simulink Diagram: The Simulink model as seen in Figure 5.25 shows the completed HVDC link operation by combining both grid side voltage sourced converter (GS-VSC) and farm side voltage sourced converter (FS-VSC) while being supplied by a constant AC current source.

Parameters used in the simulation for Farm Side: AC current source magnitude = 252.5 A;

LC Filter used for farm side: Inductance: $L = 0.001$ H and Capacitance: $C = 0.0001$ F; DC Link Capacitance $C = 0.1$ F. According to Appendix E, Farm side voltage is 132 kV and farm side power is 100 MW.

Parameters used in the simulation for Grid Side: RMS AC Grid Voltage= 132 kV and Peak AC grid voltage= $\sqrt{2}\times 132\text{ kV} = 186.676\text{ kV}$, AC Grid impedance values: $L = 1\text{ mH}$, Reference voltage for the DC Voltage Controller: $Vdc^{*} = 330\text{ kV}$. **Assumption:** In this completed HVDC system, there is a power balance between the grid side power and the farm side power (100 MW).

5.6. Simulation Results of Simulink Model - 3

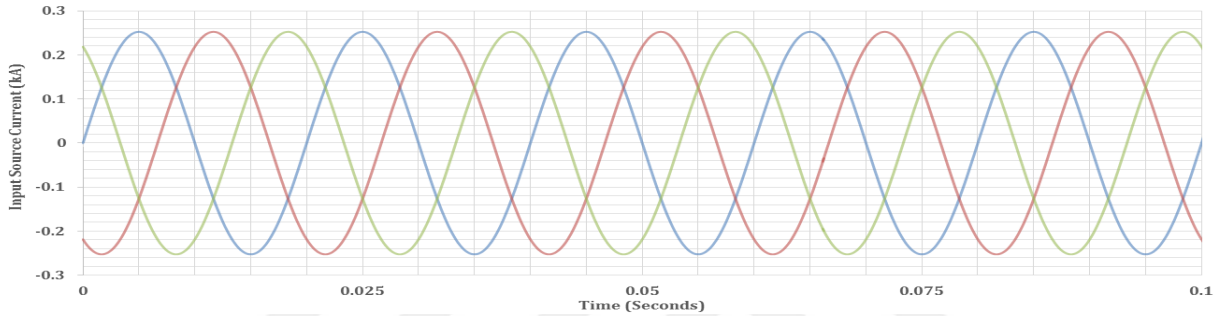

Figure 5.26: The waveform of the constant input current source used in farm side.

Comment for Input current source: Figure 5.26 shows the used constant input current source in the Simulink model, its amplitude is 252.5 A, this provides a constant current for the completed system.

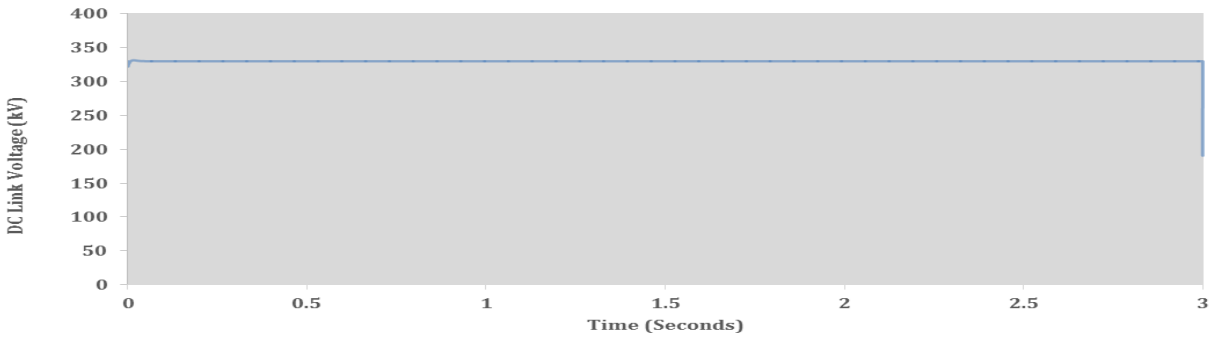

Figure 5.27: The voltage waveform across the DC side on combining GS-VSC and FS-VSC (with constant current source).

Comment for DC link voltage: Figure 5.27 demonstrates the DC Link voltage for the completed HVDC link with both GS-VSC and FS-VSC. According to the combined system, the grid side inverter supplies AC current to the utility side by keeping the system power balance. While the

power flow is being controlled in the HVDC system, the uni-directional DC Link voltage can be maintained as a constant value. It is observed that by the q axis current, the active power is controlled independently while the reactive power can be controlled by the d axis current. It is clear that as a result of the applied demand voltage to the controllers, the DC Link voltage is stabilized fast its reference voltage $(330\,\text{kV})$ in 0.5 second. It is concluded that an excellent DC voltage is obtained from the HVDC link.

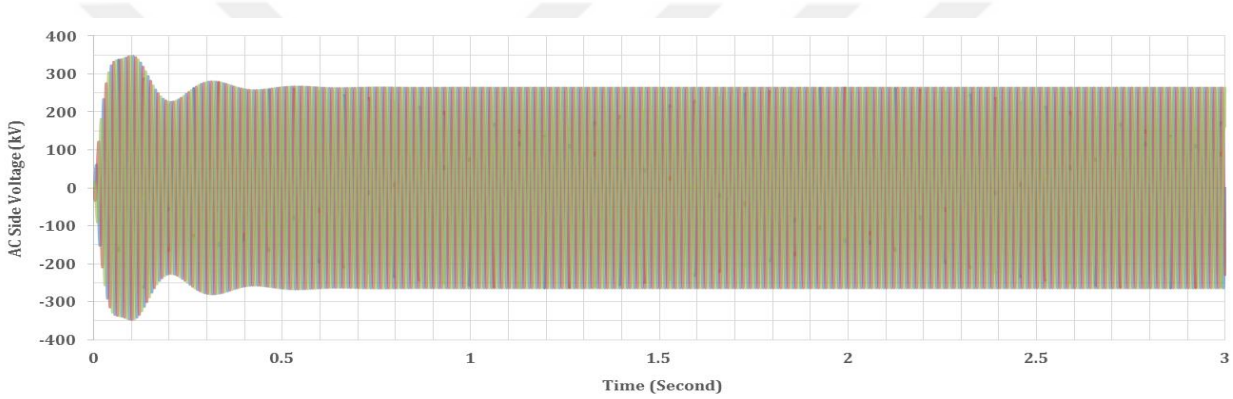

Figure 5.28: The AC side voltage waveform in the farm side (with constant input current source).

Comment for AC Voltages at the Farm side: Figure 5.28 shows the AC side voltage waveform in the farm side by using the constant input current source with its amplitude of $252.5\,\text{A}$. It is observed that there is no significant change in the voltage of AC filter which is controlled by FS-VSC after combining the FS-VSC and GS-VSC.

Comment for FS-VSC Voltage: Figure 5.29 shows the waveform of the AC voltage which is controlled by the FS-VSC as independent from the DC load size and the current source amplitude. By utilizing the AC voltage controller loop which controls the voltage drop on the AC filter capacitance, the farm Side Voltage Sourced Converter is able to control its AC grid voltage as independent from the load size and the current source.

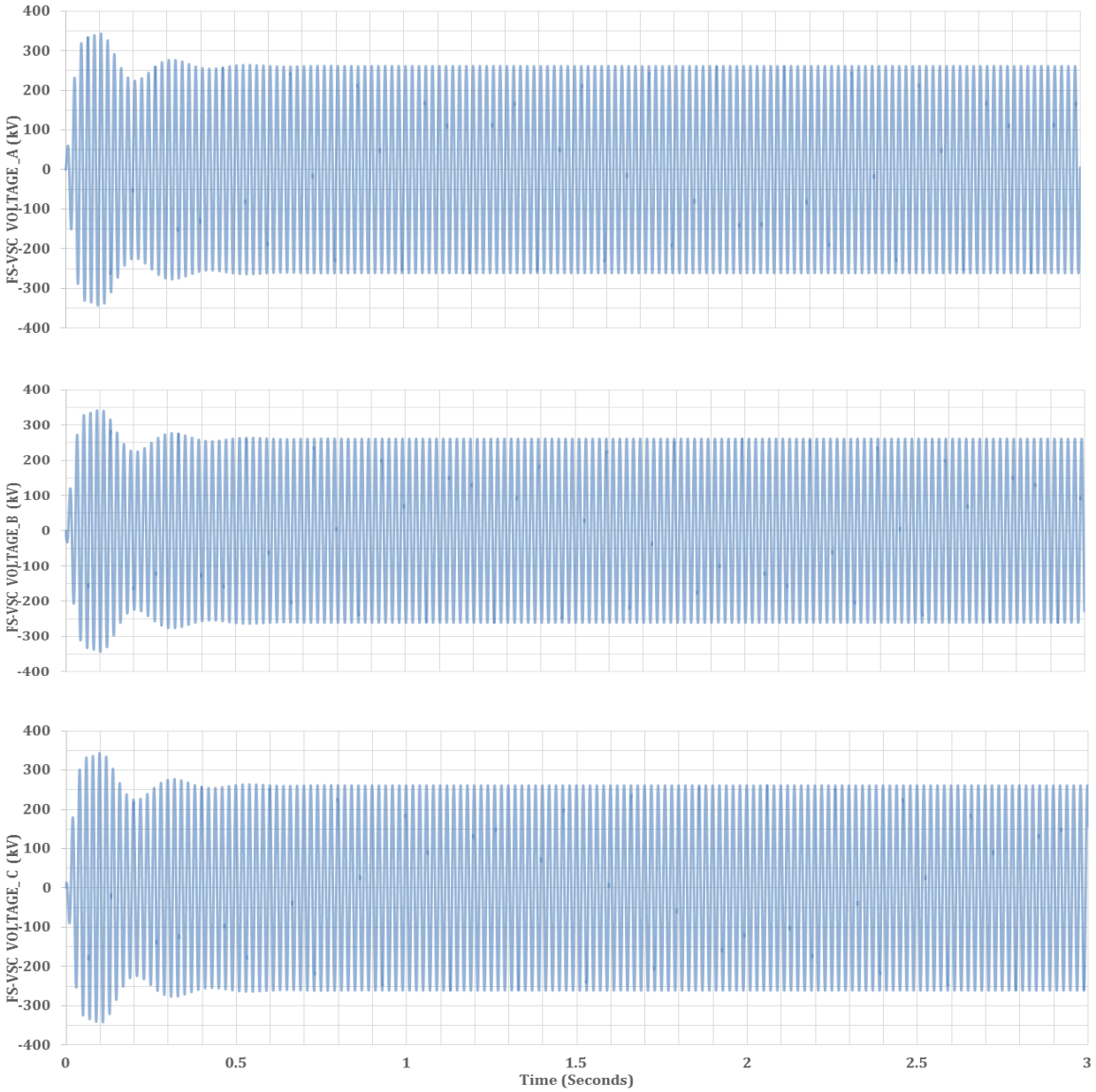

Figure 5.29: The waveforms of the AC Voltages in the Farm Side controlled by the FS-VSC.

Comment for GS-VSC Voltage: The waveforms seen in Figure 5.30 prove that GS-VSC can control the DC voltage as independent from the DC load size and the current source amplitude. By utilizing the DC voltage controller loop which controls the voltage drop on the DC side capacitance, the GS-VSC is able to control its DC link voltage as independent from the load size and the current source.

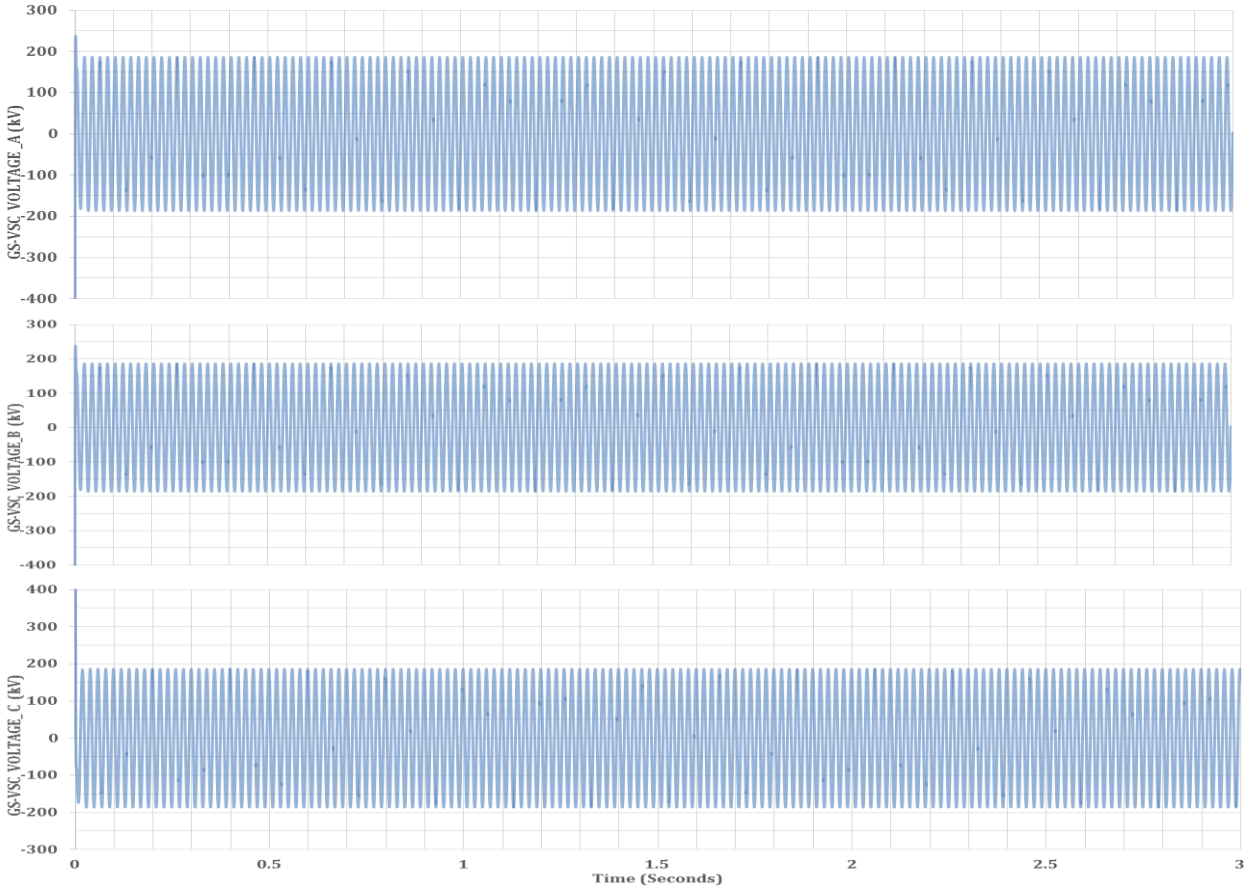

Figure 5.30: Demonstration of the DC Voltages been controlled by the GS-VSC.

Comment for DC current from GS-VSC and FS-VSC: Figure 5.31 shows the DC currents obtained from the GS-VSC and FS-VSC by utilizing the average value model principle, respectively. The demonstrated DC link currents are attained on combining the both voltage sourced converters therefore completing the VSC-HVDC link.

Comment for Farm Side and Grid Side Power: Figure 5.32 demonstrates the waveform of the Farm side power and grid side power in completed HVDC link, respectively. According to these figures, it is observed that there is a power balance between grid side voltage source converter and farm side voltage source converter. 100 MW power is maintained in the completed HVDC Link, therefore it is concluded that there is no power losses at the both grid side and farm side in the HVDC Link.

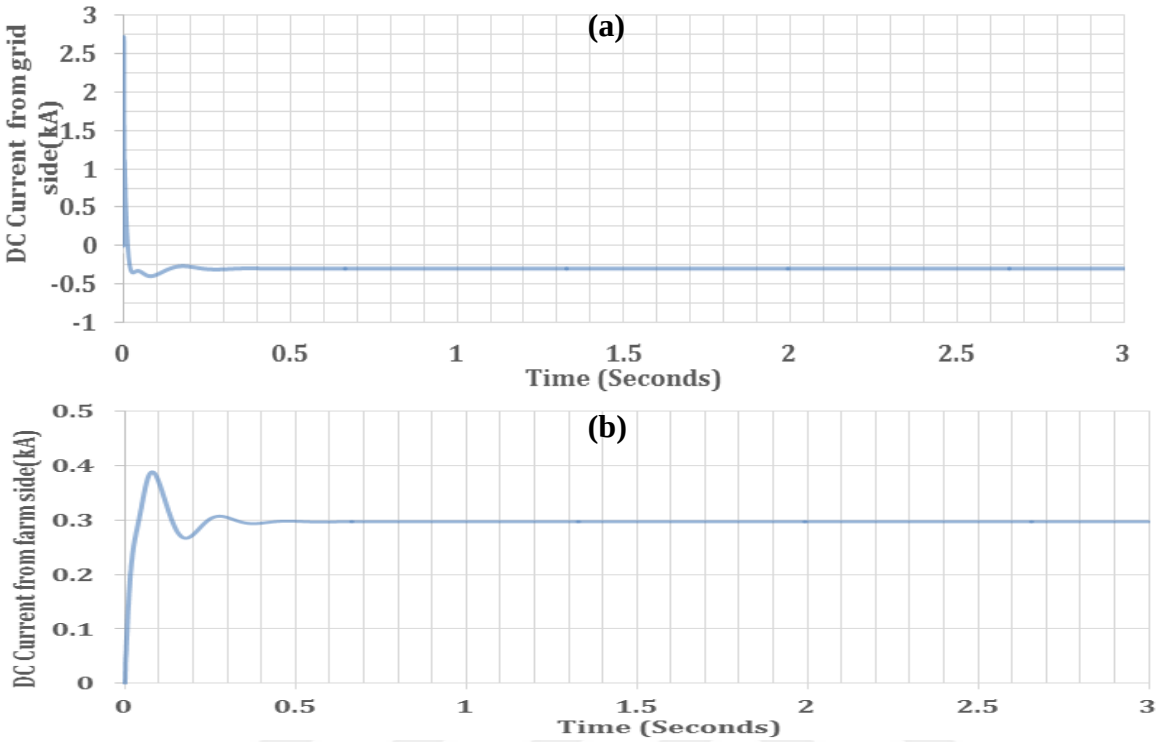

Figure 5.31: The waveform of the DC current attained from; (a) GS-VSC and (b) FS-VSC when the HVDC system is fed by a constant AC current source.

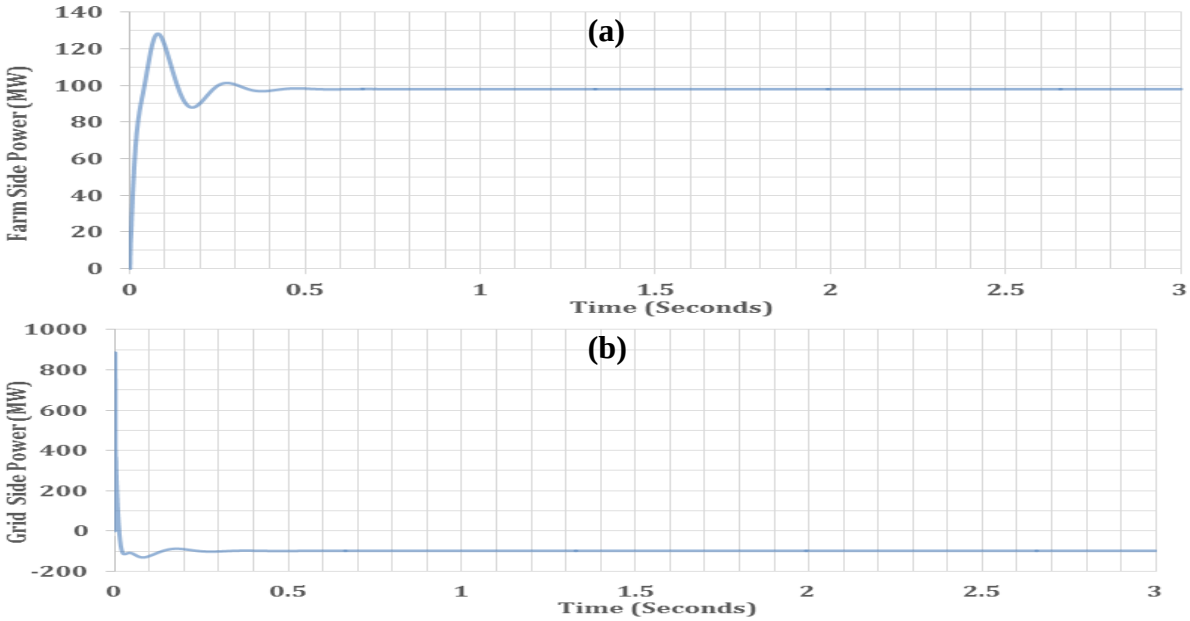

Figure 5.32: The demonstration of the (a) Farm and (b) Grid Side Power in the HVDC Link.

5.7 Matlab Simulink Model-4

Objective: The aim of this model is to attach the average model of the wind farm to the HVDC link utilizing the wind farm data as seen in Appendix A and illustrate the system operation under changing wind speeds and for a phase to ground fault on the grid side.

Powergui Parameters: Discrete: $5e-05$ sec. **Wind Farm:** 100 MW Average Model DFIG based wind turbine (wind farm parameters are shown in Appendix A). Wind Turbine: wind turbine numbers = 67 and nominal power rate=$1.5e6/0.9$ Wind Speed: Variable wind speeds from 11 m/s to 15 m/s. Stator Side Transformer parameters are shown in Appendix A.

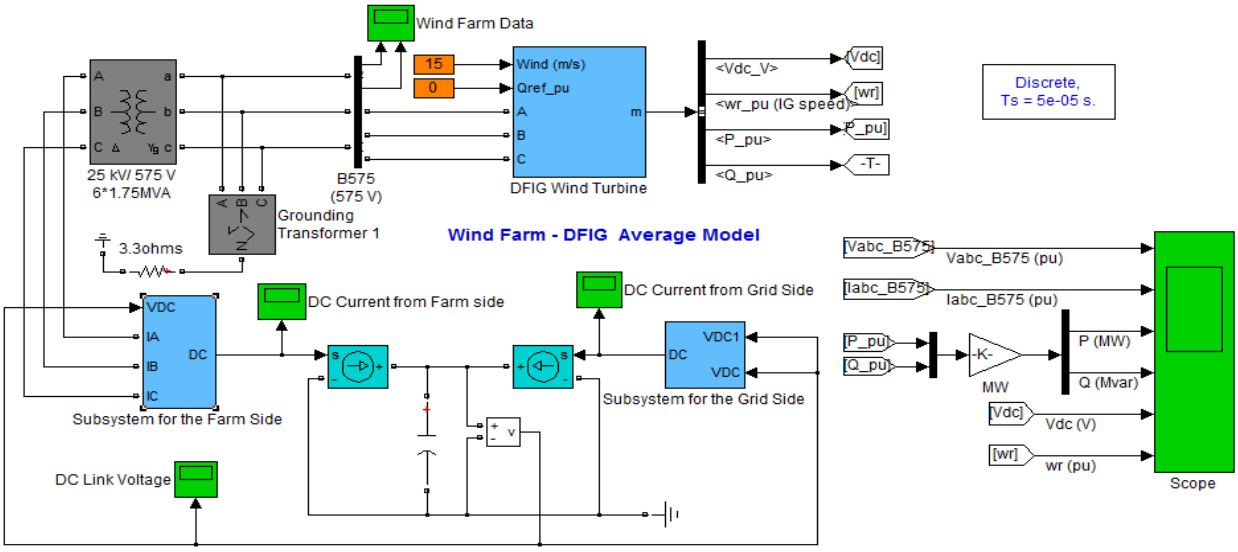

Figure 5.33: The HVDC Link with the average model of the DFIG based wind farm.

5.7.1 Case 1: The operation of the completed HVDC system is demonstrated under variable wind speeds.

Simulink Model: Figure 5.33 shows the operation of the HVDC system when the average model of the DFIG based wind farm is attached to the whole HVDC system under changing wind speeds.

5.7.2 Simulation Results of Simulink Model – 4 Case 1

Comment for Current and Voltage from wind farm: Figure 5.34 shows the waveforms of the obtained current and voltage output from the average model of the DFIG based wind farm. The output of the wind farm acts to the HVDC system as a variable current source. From the simulation, the expected current and voltage of 80A and around 100kV are successfully obtained, respectively.

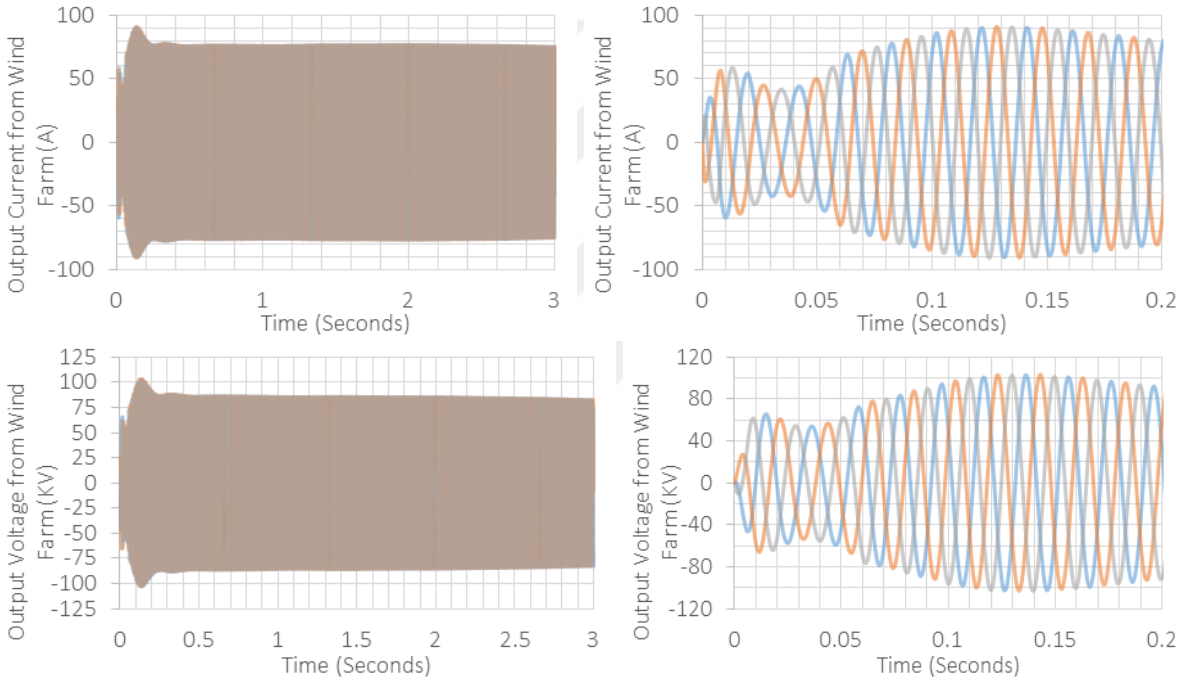

Figure 5.34: The waveform of the output current and voltage from the average model of the DFIG based wind turbine.

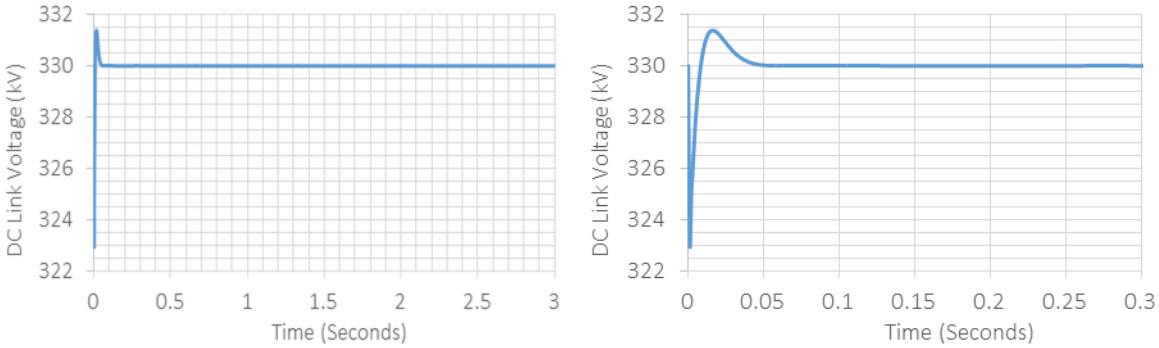

Figure 5.35: The waveform of the DC Link Voltage when the wind farm acts as a current source to the HVDC system.

Comment for DC Link Voltage: Figure 5.35 illustrates the DC side voltage waveform. It is observed that due to the $330\,\text{kV}$ of a demand voltage is applied to the voltage controller, on the DC link, an excellent DC voltage is obtained from the voltage controller (PI controller) on the GS-VSC control design. According to this graph, a voltage transient is shown by 0.1 second, but the DC link voltage is able stabilized fast to its reference voltage value by the PI control.

Comment for Grid side AC current: Figure 5.36 shows the three-phase AC current waveform on the grid side when the average model of the DFIG based wind farm is connected to the HVDC link. It is clear that the grid side AC current shows a stability with an around $3800A$ current magnitude for the $132kV$ of single phase AC voltage. It is resulted that an excellent stable three-phase grid side current is obtained from the simulation after responding a transient in around 0.02 second.

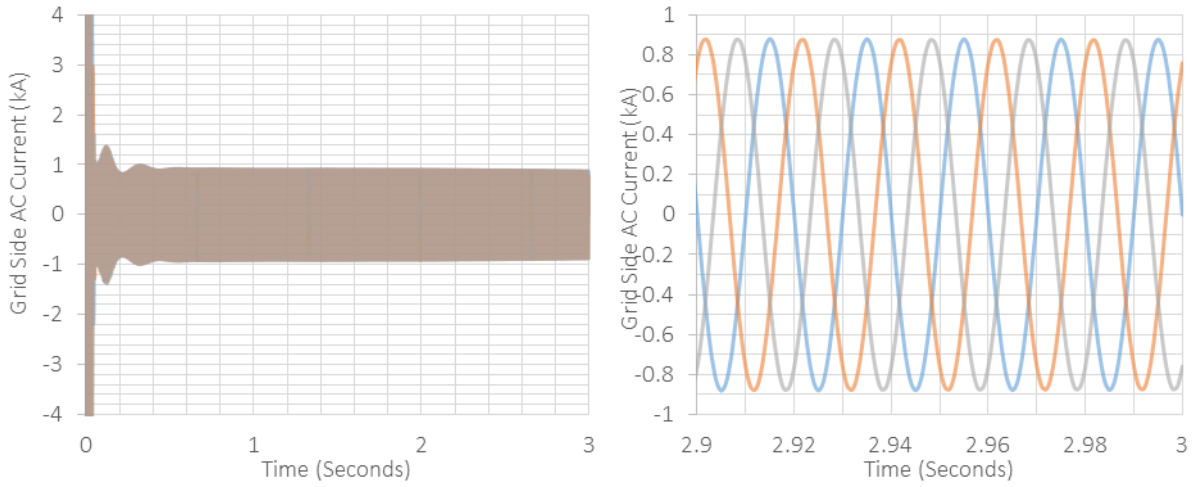

Figure 5.36: The waveform of the grid side current when the wind farm acts as a current source to the HVDC system.

Comment for DC link current from farm and Grid Side: Figure 5.37 demonstrates the DC link currents attained from the grid side and farm side voltage source converter with the average model method. It is observed that these DC link currents respond to the transient fast and maintains to its constant value.

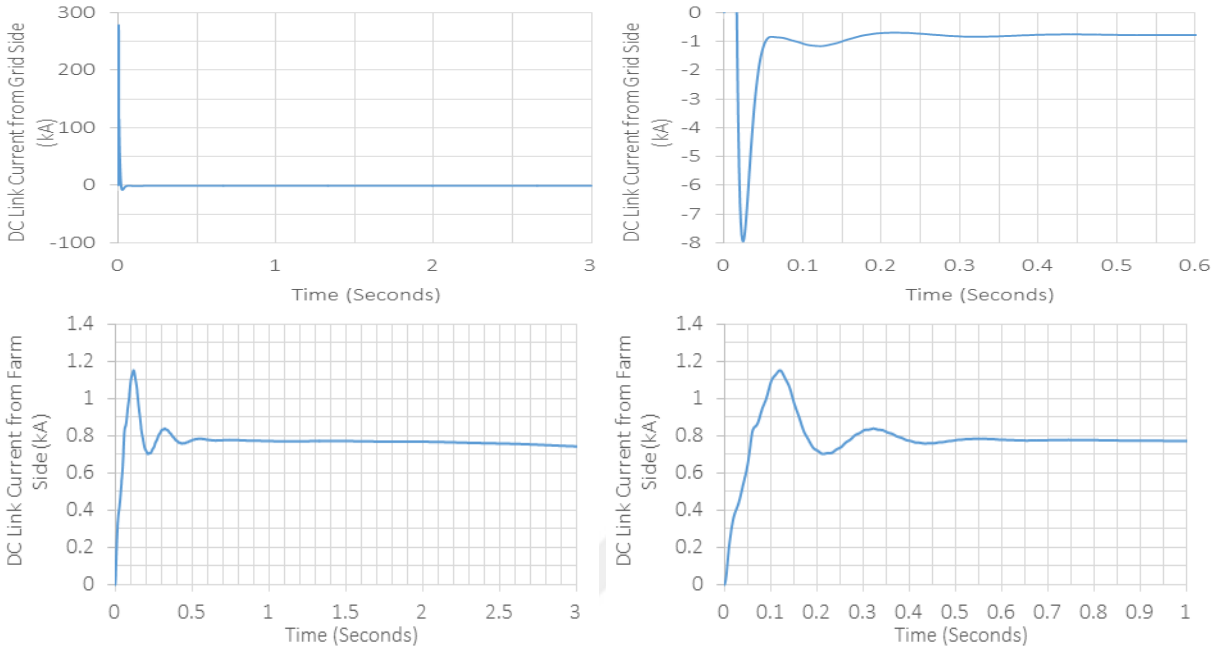

Figure 5.37: DC Link Currents from Farm and Grid Sides.

5.7.3 Case 2: To demonstrate the completed HVDC link operation when the average model of the DFIG based wind farm is attached to the HVDC system for the situation of a phase to ground fault on the grid side.

Figure 5.38 illustrate the Simulink diagram when the average model of the DFIG based wind farm is connected to the completed HVDC link so as to demonstrate its operation for a phase to ground fault on the grid side.

Simulation Parameters: Phase to phase AC grid voltage=132 kV, frequency= 50 Hz, source resistance = 0.1 Ω, Ground resistance for phase A to ground fault = 0.001 Ω. Three-phase parallel load on the grid side $R = 100\ \Omega$ and $L = 1e-5$ H. Snubber resistance =1e6 Ω, Transition time (s): [1.5 2].

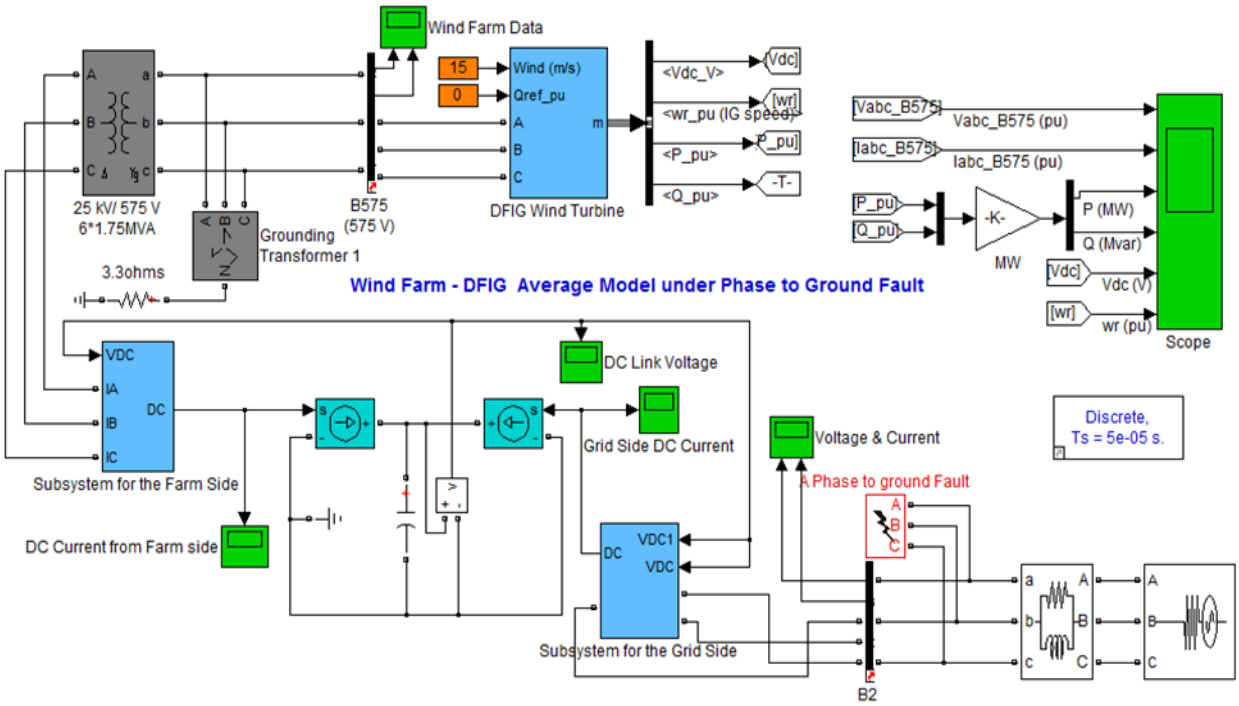

Figure 5.38: The HVDC system with DFIG wind farm for a phase to ground fault on the grid side.

5.7.4 Simulation Results of Simulink Model – 4 Case 2

Comment for Grid side AC current and AC voltage: The waveforms as seen in Figure 5.39 shows the grid side current and voltage on the existence of a phase to ground fault, respectively. It is observed that in a transition time of 1.5 to 2 seconds. A phase A to ground fault occurs on the grid side. This fault affects the both AC current and AC voltage waves. However, these waves show a recovery after 2 seconds of transition time and therefore maintains its stability.

Comment for DC Voltage: The waveform as seen in Figure 5.40 demonstrates the obtained DC link voltage when a phase A to ground fault occurred on the AC side in a transient time of 1.5 to 2 seconds. Due to the performance of the voltage controller in the grid side, the DC link voltage is able to keep its magnitude of 330kV which is determined as the reference voltage for the voltage controller after the fault transmission.

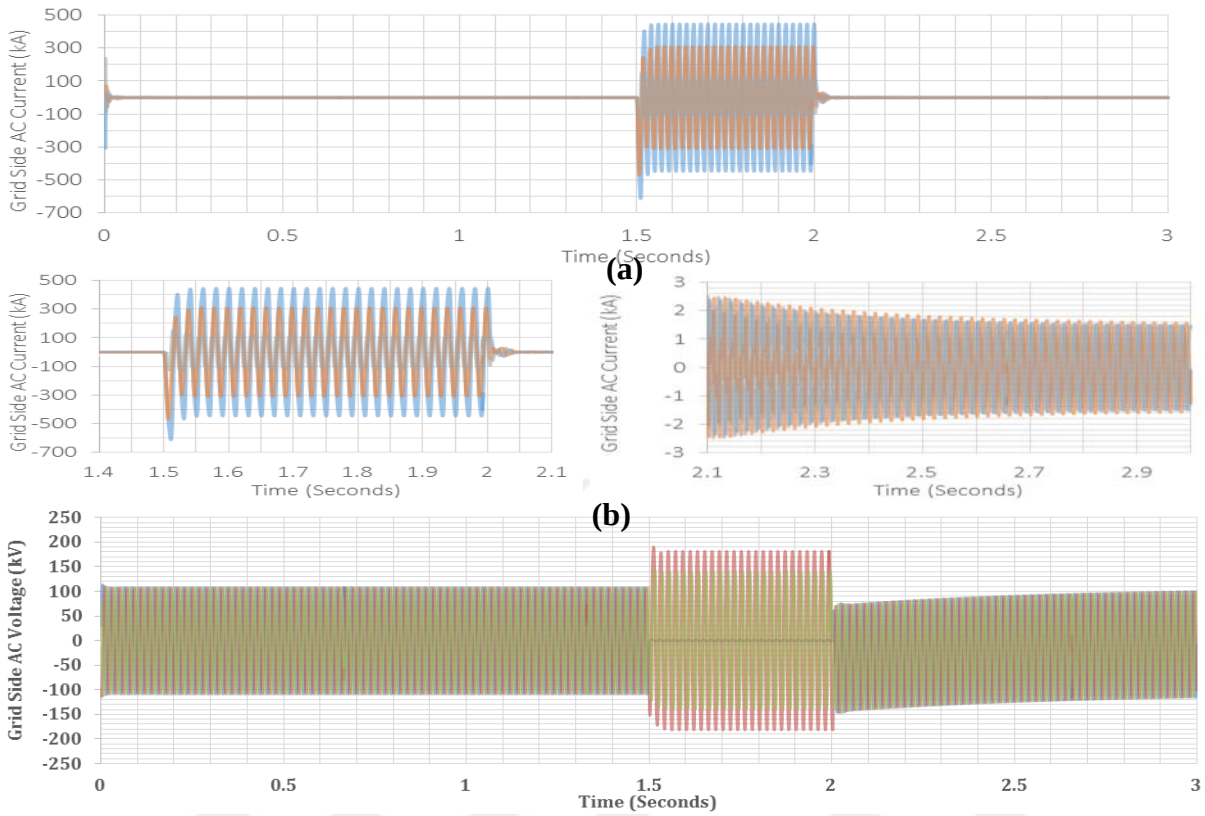

Figure 5.39: The waveform of the grid side (a) currents and (b) voltages on the existence of a fault.

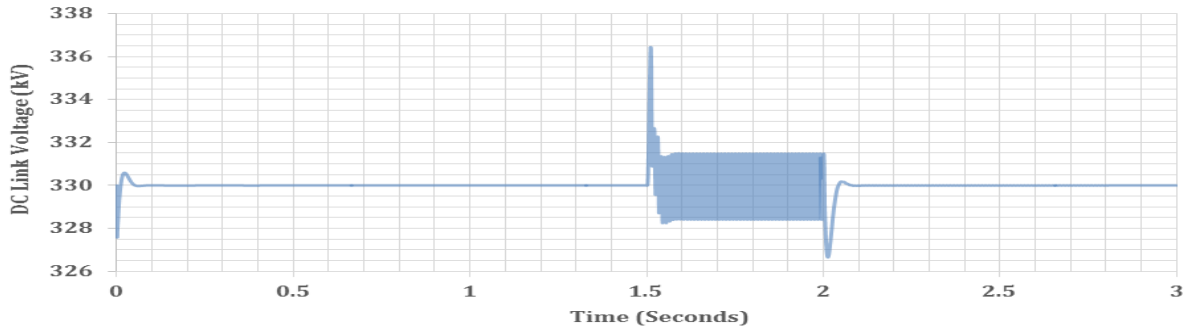

Figure 5.40: The waveform of the DC link voltage on the existence of a fault.

Comment for DC Current: Figure 5.41 shows the waveform of the DC link current when a phase to ground fault occurs on the grid side in the transition time of 1.5 to 2 seconds. It is clear that the wave of the DC current is able to maintain its value which has around 770 A magnitude after the fault transition.

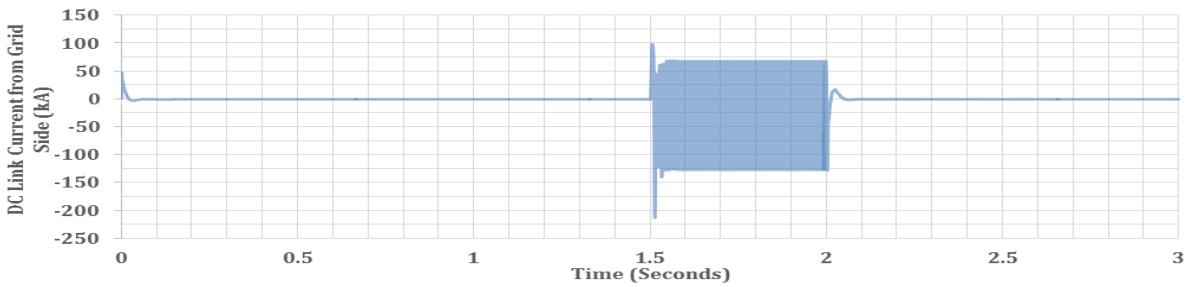

Figure 5.41: The waveform of the DC link voltage on the existence of a fault.

5.8 Matlab Simulink Model - 5

Objective: To construct the CIGRE 12 bus bench mark model with given data as seen in Appendix B and demonstrate the system operation for load and wind speed variations and for a fault on Bus1. Powergui Block Parameters: Discrete, $5e-05$ sec. Wind Farm parameters used in Simulink is shown in Appendix A. Wind Farm Model Type: $100\,MW$ Average Model DFIG based Wind Turbine. Wind Turbine Data: The no.of wind turbines are 67 with nominal power rating of $1.5e6/0.9$. Wind Speed Data: The initial wind speed is $11\,m/s$ and varied up to $15\,m/s$. CIGRE 12 bus bench mark system data used for the Simulink diagram is shown in Appendix B which describes load and capacitor parameters, transmission line data, transformer data and generator data to show the performance of CIGRE 12 bus system. It is noted that Transmission line parameters are shown in Table 2, Appendix B as well as Table 2A which describes the conversion of the per unit quantities to its real values with considering its base MVA.

Case 1: To demonstrate the performance of the CIGRE 12 bus bench mark model for load variations and wind speed variations.

Load variations implemented to the CIGRE 12 bus system:

- **At Bus 2:** Active Power P = 280 MW and Inductive Reactive Power QL = 200 Mvar,

- **At Bus 3:** Active Power P = 320 MW and Inductive Reactive Power QL = 240 Mvar,
- **At Bus 4:** Active Power P = 320 MW and Inductive Reactive Power QL = 240 Mvar with Capacitive reactive Power QC = 120 Mvar,
- **At Bus 5:** Active Power P = 320 MW and Inductive Reactive Power QL=240 Mvar with Capacitive reactive Power QC = 120 Mvar,

The Connected Generators data at the CIGRE 12 bus system:

G2: 588 MVA, 22 kV of synchronous machine, connected load = 10 kW, **G3:** 235 MVA, 22 kV of synchronous machine, connected load = 10 kW, **Wind Speed variations implemented to the system:** Initial wind speed is 11 m/s and varied up to 15 m/s. The Simulink diagram as seen in Figure 5.42 shows the complete CIGRE 12 bus bench mark model with respect to the data given in Appendix B. Figure 5.42: CIGRE 12 bus bench mark system.

Case 2: To demonstrate the performance of the CIGRE 12 bus bench model for **a fault on Bus 1.** The Simulink diagram as seen in Figure 5.43 shows the complete CIGRE 12 bus bench mark model for a phase to ground fault on Bus1.

Simulink Parameters used in system: Transition status= [1 0]; transition times= [1/60 5/60]; Fault resistance and ground resistance= $0.001\ \Omega$ Figure 5.43: CIGRE 12 bus bench mark system for a phase to ground fault on Bus 1.

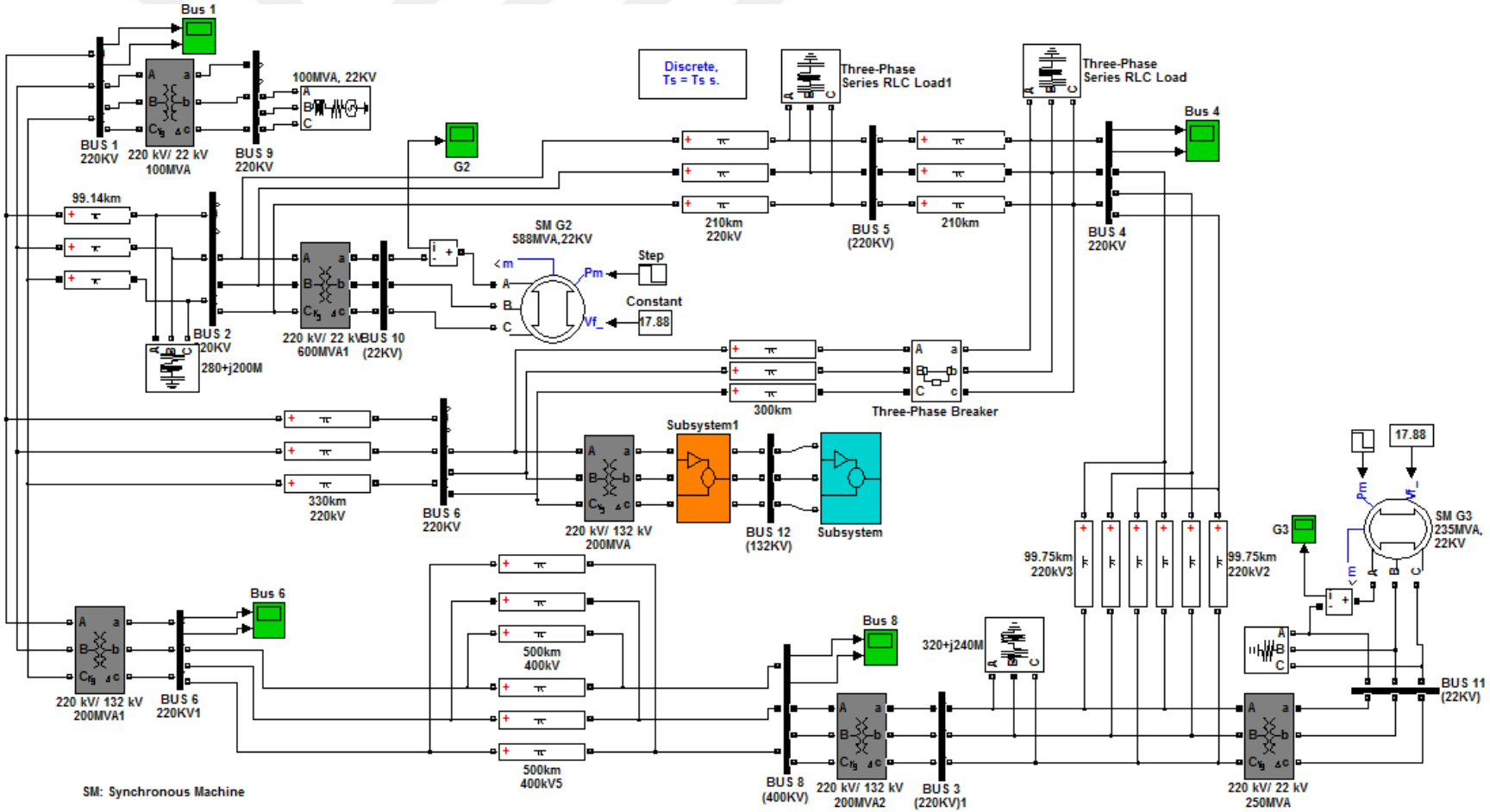

Figure 5.42: Complete CIGRE 12 bus bench mark model.

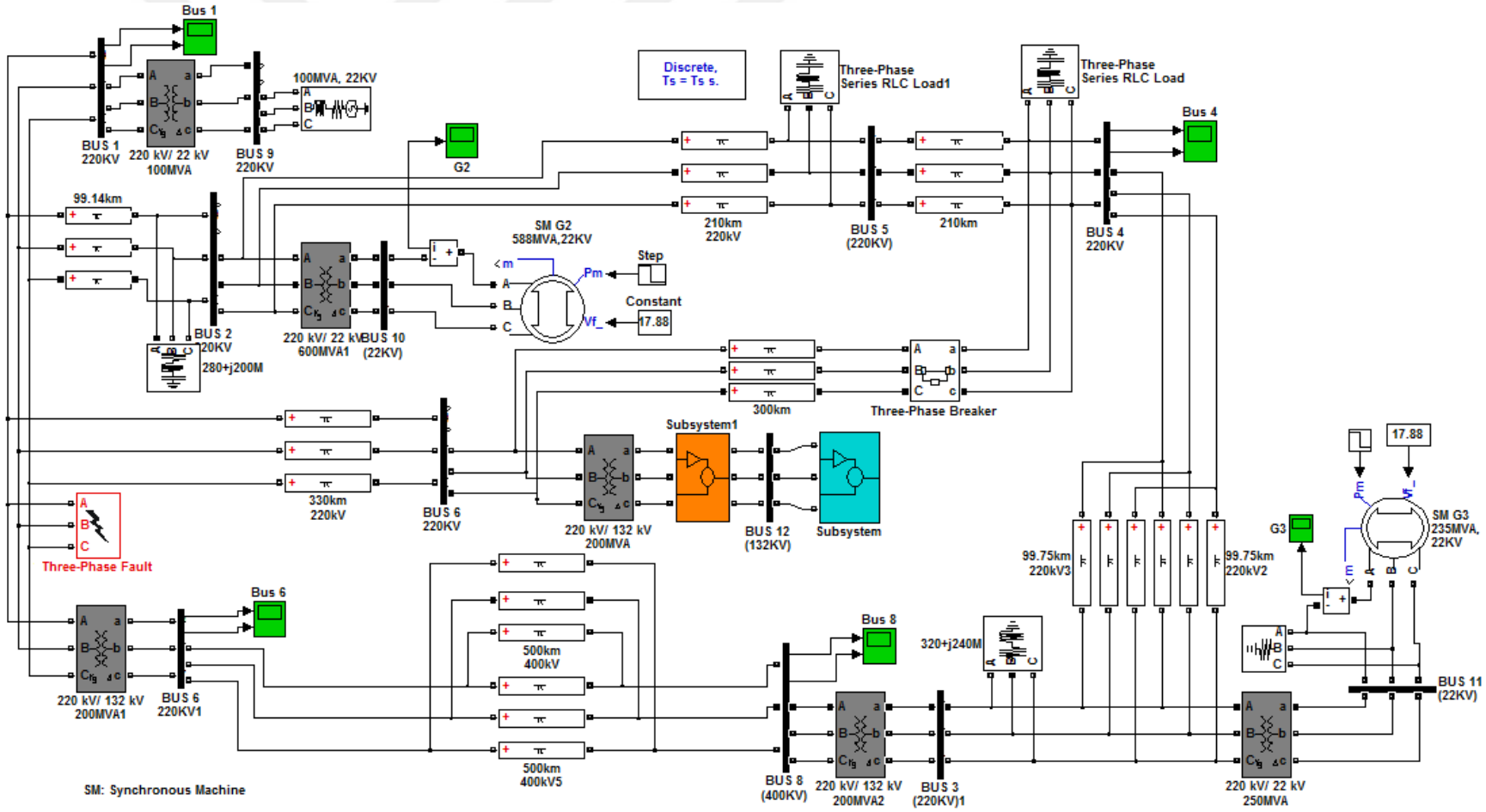

Figure 5.43: Complete CIGRE 12 bus bench mark model for a phase to ground fault on Bus1.

Conclusions

The main task of this thesis is to understand and examine the behavior of the voltage sourced converter based high voltage direct current (VSC-HVDC) transmission system. This report is structured into five chapters therefore providing us to have good understanding for the system. The major stage of the modelling of the VSC-HVDC system is presented in this project.

The control strategy of the HVDC system is based on a fast inner control loop for the control of the AC current through and outer voltage controller. Utilizing the average model concept of the VSC, the PI controller method is formed for the outer and inner control loops in the synchronous reference frame. The transformation of the abc co-ordinates to the synchronous reference frame for the extraction of the phase angle were presented as a general guidelines.

This thesis is mainly utilized Matlab Simulink models for the VSC-HVDC system by analyzing the overall system operation separately for the grid side and farm side. The HVDC system was analyzed with the average model of the DFIG based wind farm in order to study its control under variable wind speeds and for fault ride through. In last stage, a 50 Hz CIGRE 12 bus bench mark system along with the complete HVDC system was modelled. According to the literature, owing to the complexity of the wind farm and HVDC system, it is not possible to model it using complete models of the switching devices. A complete DFIG wind farm model with controls is already provided in the MATLABSimPowerSystems toolbox, however a non-switching phasor model of a voltage source converter is not available in there. Hence, this thesis is concentrated to construct the non-switching phasor model of VSC and a suitable control scheme for the HVDC link. It is concluded that a fast system response and an accurate control for the HVDC link is achieved to a certain level.

Bibliography

[1] P. Bresesti, W. L.Kling, R. L.Hendriks and R. Vailati, "HVDC Connection of Offshore Wind Farms to the Transmission System," *IEEE Transactions on Energy Conversion,* vol. 22, no. 1, p. 37, March 2007.

[2] S.K.Chaudhary, R.Teodorescu and P.Rodriguez, "Wind Farm Grid Integration Using VSC Based HVDC Transmission- An Overview," in *IEEE Energy2030*, Atlanta,GA USA, 17-18 November 2008.

[3] C. Nicolle, "Offshore Wind Farms," Coastal and Ocean Engineering Undergraduate Student Forum, Canada, March 2013.

[4] R. UK, "Offshore Wind Energy," 11-12 June 2014. [Online]. Available: http://www.renewableuk.com/en/renewable-energy/wind-energy/offshore-wind/.

[5] R. Rudervall, J. Charpentier and R. Sharma, "High Voltage Direct Current (HVDC) Transmission Systems Technology Review Paper," in *Energy Week 2000*, Washington, D.C, USA, March 7-8, 2000.

[6] N. Flourentzou, V. G.Agelidis and G. D.Demetriades, "VSC-Based HVDC PowerTransmission Systems: An Overview," *IEEE Transactions on Power Electronics,* vol. 24, no. 3, p. 592, March 2009.

[7] O.A.Giddani, G.P.Adam, O.Anaya-Lara and G.-B. a. K.L.Lo, "Control Strategies of VSC-HVDC Transmission System for Wind Power Integration to Meet GB Grid Code Requirements," in *SPEEDAM 2010 International Symposium on Power Electronics,Electrical Drives,Automation and Motion*, 2010.

[8] ABB, "HVDC," [Online]. Available: http://new.abb.com/systems/hvdc.

[9] D. Watson, "FACTS Lecture notes: HVDC Transmission Background and Concepts," The University of Nottingham, 2014.

[10] J. Wu, Z.-X. Wang, L. Xu and G.-Q. Wang, "Key technologies of VSC-HVDC and its application on offshore wind farm in China," *ELSEVIER,* vol. 36, p. 247–255, August 2014.

[11] M. Bahrman and P.E., "HVDC Transmission Overview," in *IEEE*, 2008.

[12] "The Gotland HVDC Link," ABB, [Online]. Available: http://new.abb.com/systems/hvdc/references/the-gotland-hvdc-link.

[13] K.R.Padiyar, HVDC Power Transmission System Technology and System Interactions, New Delhi: New Age International (P) Limited, 2005.

[14] M. Larsson, "HVDC and HVDC Light An alternatif power transmission system," in *Symposium on Control & Modelling of Alternative Energy Systems*, April 2,2009.

[15] C. Du, "The Control of VSC-HVDC and its use for large industrial power systems," Chalmers University of Technology, Sweden, 2003.

[16] E. K. Amankwah, "A Parallel Hybrid Modular Multilevel Converter for High Voltage DC Applications," The University of Nottingham, Nottingham, August,2013.

[17] "HVDC Plus (VSC Technology)," Siemens, [Online]. Available: http://www.energy.siemens.com/us/en/power-transmission/hvdc/hvdc-plus/.

[18] K. Meah and S. Ula, "Comparative Evaluation of HVDC and HVAC Transmission System".

[19] "Economic and Environmental Advantages," ABB, [Online]. Available: http://new.abb.com/systems/hvdc/why-hvdc/economic-and-environmental-advantages.

[20] H. Wang and M.A.Redfern, "The advantages and disadvantages of using HVDC to interconnect AC networks," in *UPEC2010*, 31st August-3rd September2010.

[21] D. Thomas, "The University of Nottingham HVDC Link Lecture Notes," The University of Nottingham, Nottingham, 2014.

[22] T. W. Shire, "VSC-HVDC based Network Reinforcement," Delft University of Technology, May 2009.

[23] S. h. J, S. G. N, Ramesh.E, D. L. N and Nataraja.C, "Voltage Source Converter Based HVDC Transmission," *International Journal of Engineering Science and Innovative Technology (IJESIT),* vol. 1, no. 1, p. 97, September 2012.

[24] C. DU, "VSC-HVDC for Industrial Power Systems," Chalmers University Of Technology, Goteborg, Sweden, 2007.

[25] S. ZHOU, "Modelling and Control of Multi-Terminal HVDC Networks for Offshore Wind Power Generation," Cardiff University, Cardiff, Wales, UK, 2011.

[26] K. Friedrich, "Modern HVDC PLUS application of VSC in Modular Multilevel Converter Topology," in *IEEE*, 2010.

[27] G. Reed, M. Takeda and R. Pape, "Advantages of Voltage Sourced Converter (VSC) Based Design Concepts for FACTS and HVDC-Link Applications," in *IEEE*, 2003.

[28] "Control Of Vsc-Based Hvdc Transmission System For Offshore Wind Power Plants," Aalborg University, Denmark, Semester, 2010.

[29] V. K. S. G.-S. J. S.-J. L. a. S.-J. L. Chan-Ki Kim, HVDC TRANSMISSION Power Conversion Applications in Power Systems, John Wiley & Sons (Asia) Pte Ltd, 2009.

[30] T. M. Haileselassie, "Control, Dynamics and Operation of Multi-terminal VSC-HVDC Transmission Systems," Norwegian University of Science and Technology, Trondheim, December 2012.

[31] E. Kontos, "Control and Protection of VSC-based Multi-terminal DC Networks," Delft University of Technology, Delft, the Netherlands.

[32] Z. Zhou, "Co-ordination of Converter Controls and an Analysis of Converter Operating Limits in VSC-HVdc Grids," The University of Manitoba, Winnipeg, Manitoba, Canada, 2013.

[33] A. Hilawie, "Investigation Of Vsc-Hvdc System For Dynamic Performance Improvement Of Eepco High Voltage Grid," Addis Ababa University, Addis Ababa, June 2011.

[34] M. S. Chinthavali, "Silicon Carbide GTO Thyristor Loss Model for HVDC Application," University of Tennessee, Knoxville, 2003.

[35] A. K. AGRAWAL, B. MUNSHI and S. KAYAL, "STUDY OF WIND TURBINE DRIVEN DFIG USING AC/DC/AC CONVERTER," National Institute of Technology Rourkela.

[36] L. Wang and K.-H. Wang, "Dynamic Stability Analysis of a DFIG-Based Offshore Wind Farm Connected to a Power Grid Through an HVDC Link," *IEEE TRANSACTIONS ON POWER SYSTEMS*, vol. 26, no. 3, p. 1501, AUGUST 2011.

[37] L. Xu, L. Yao and C. Sasse, "Grid Integration of Large DFIG-Based Wind Farms Using VSC Transmission," *IEEE TRANSACTIONS ON POWER SYSTEMS*, vol. 22, no. 3, p. 976, AUGUST 2007.

[38] G. Asplund, K. Eriksson and K. Svensson, "DC Transmission based on Voltage Source Converters," in *CIGRE SC14 Colloquium*, South Africa, 1997.

[39] N. D. Aldana, C. L. Trujillo and J. G. Guarnizo, "Active and reactive power flow regulation for a grid connected VSC based on fuzzy controllers," *Rev. Fac. Ing. Univ. Antioquia*, vol. 66, pp. 118-130, 2013.

[40] K. MOHAMED, Z. S. AHMED, H. SAMIR, F. M. KARIM and A. RABIE, "Performance Analysis of a Voltage Source Converter (VSC) based HVDC Transmission System under Faulted Conditions," Djillali

Liabes University, Algeria.

[41] entsoe,"Offshore Transmission Technology," 2011. [Online]. Available: https://www.entsoe.eu/fileadmin/user_upload/_library/publications/entsoe /SDC/European_offshore_grid_-_Offshore_Technology_-_FINALversion.pdf.

[42] S. Ruihua, Z. Chao, L. Ruomei and Z. Xiaoxin, "VSCs based HVDC and its control strategy," in *2005 IEEE/PES Transmission and Distribution*, Asia and Pacific Dalian,China, 2005.

[43] H. Ouquelle, L.-A. Dessaint and S.Casoria, "An Average Value Model-Based Design of a Deadbeat Controller for VSC-HVDC Transmission Link," in *IEEE*, 2009.

[44] W. Yao, J. Wen, H. He and S. Cheng, "Modelling and Simulation of VSC-HVDC with Dynamic Phasors," in *DRPT2008*, Nanjing China, 6-9 April.

[45] J. Peralta, H. Saad, S. Dennetiere and J. Mahseredjian, "Dynamic Performance of Average-Value Models for Multi-terminal VSC-HVDC Systems," in *IEEE*, 2012.

[46] H. Patel, "Modeling of Voltage Source Converter Based HVDC Transmission System in EMTP-RV," University of Ontario Institute of Technology, August, 2010.

[47] R. Pena, J.C.Clare and G. M. Asher, "Doubly fed induction generator uising back-to-back PWM converters and its application to variablespeed wind-energy generation," *IEE Proc.-Electr. Power Appl.*, vol. 143, no. 3, p. 231, May 1996.

[48] Y. Liu, X. Wang and Z. Chen, "Cooperative Control ofVSC-HVDC Connected Offshore Wind Farm with Low-Voltage RideThrough Capability," in *IEEE*, 2012.

[49] M. M. Hussein, T. Senjyu, M. Orabi, M. A. A. Wahab and M. M. Hamada, "Control of a Stand-Alone Variable Speed Wind Energy Supply System," *Applied Sciences*, vol. 3, no. 2, pp. 437-456, 2013.

[50] G. F. Pla and A. G. Matias, "Control of grid side inverter for wind turbine," Aalborg Universitet, 2010.

[51] S. R. Nandurkar and M. Rajeev, "Design and Simulation of three phase Inverter for grid connected Photovoltic systems," in *Proceedings of Third Biennial National Conference, NCNTE*, 2012, Feb 24-25.

[52] R. Leelaruji, "Availability Assessment of HVDC Converter Transformers Using Markov Modelling," KTH Electrical Engineering, April 2007.

[53] R. T. P. R. R. da Silva, "Power Delivery in Multiterminal VSC-HVDC Transmission System for Offshore Wind Power Applications," in *Innovative Smart Grid Technologies Conference Europe (ISGT Europe), 2010 IEEE PES*, Gothenburg.

[54] T. Gundogdu and G. Komurgoz “Technological and Economical analysis of salient pole and permanent magnet synchronous machines designed for wind turbines” Elsevier Journal of Magnetism and Magnetic Materials, vol.324, pp. 2679-2686, Dec. 2012

[55] T. Gundogdu and G, Komurgoz “Implementation of fractional slot concentrated winding technique to large salient-pole synchronous generators & development with permanent magnets, Electric Power Systems Research, Vol. 105, pp. 57–70, Dec. 2013.

[56] T.Gundogdu and G, Komurgoz, “Self-tuning PID control of a brushless DC motor by adaptive interaction”, IEEJ Transactions on Electrical and Electronic Engineering, Vol. 9-4, pp. 384–390, July 2014.

[57] T.Gundogdu, G.Komurgoz and B.Mantar, “Design of SPSGs with Fractional-Slot Concentrated Windings and Comparison over Conventional SPSGs”, the IASTED International Symposium on Power and Energy (IASTED PE’13), Nov. 2013, Marina Del Rey/USA.

Appendix A: Wind Farm Model data

The DFIG parameters used in **Matlab Simulink Model-4** are given in Table A1.

Table A1: DFIG parameters.

Parameter	**Value**	**Parameter**	**Value**
Rated Power	100MW	Stator resistance	0.0066 [pu]
Rated Voltage (Line to Line	1 kV	Rotor resistance	0.0044 [pu]
Base Angular Frequency	314.159rad/sec	Magnetizing inductance	3.07 [pu]
Stator/Rotor Turns ratio	1	Stator leakage	0.07 [pu]
Angular moment of inertia	2 Sec.	Rotor leakage inductance	0.15 [pu]
Mechanical damping	0.01 [pu]		

DC link capacitor rating = 0.1 F, Dc link voltage rating = 2 kV. Parameters for the stator side transformer: A Y-Y 200 MVA transformer was connected between the stator and the grid and the parameters are: Frequency = 50 Hz, Leakage reactance = 0.12 [pu], winding 1 line to line RMS Voltage = 1 kV, winding 2 line to line Voltage (RMS) = 33 kV. Parameter for the rotor side decoupling transformer: Transformer type is Y-Y 40MVA, Frequency = 50 Hz, Leakage reactance = 0.12 [pu], Resistance = 0.05 [pu], winding 1 line to line RMS Voltage = 1 kV, winding 2 line to line Voltage (RMS) = 33 kV.

Appendix B: CIGRE 12 bus bench mark model data

Table B1: Load and Capacitor parameters for CIGRE 12 bus system.

Bus Number	Active Load [MW]	Inductive Load [MVar]	Shunt Capacitance [MVar]
2	280	200	-
3	320	240	-
4	320	240	120

5	100	60	80
Total	1020	740	200

The positive line sequence parameters for the transmission line based on 100MVA are presented in Table B2.

Table B2: Transmission line data for CIGRE 12 bus system.

Line	Nominal	Length [km]	Resistance	Reactance	Susceptance
1-2	220	99.14	0.0123	0.0782	0.146
1-6	220	300	0.0360	0.2330	0.445
2-5	220	210	0.0257	0.1650	0.310
3-4 (line 1)	220	99.75	0.0124	0.0787	0.147
3-4 (line 2)	220	99.75	0.0124	0.0787	0.147
4-5	220	210	0.0257	0.1650	0.310
4-6	220	300	0.0360	0.2330	0.445
7-8 (line 1)	400	500	0.0087	0.0900	3.152
7-8 (line 2)	400	500	0.0087	0.0900	3.152

The transmission line data is given in per unit values based on 100MVA. But in the Simulink diagram, the conversion has to be made as below so as to obtain the actual values implemented as the Simulink parameters. The per unit value = the actual value / the base or reference value. The base impedance is given by: $\frac{Vb*Vb}{Sb}$, where Vb is the base voltage = 22KV and Sb is the base VA = 100 MVA. Hence the actual values of Resistances / Reactance / Susceptance are computed as below:

[(Rpu / Xpu / Bpu)* (Vb*Vb)] / Sb

The Table 2A illustrates the actual values for the resistances, reactance and susceptance respectively which is been computed by using Table B3.

Table B3: Transmission Line Data for the CIGRE 12 Bus System.

Line	Nominal Voltage (KV)	Length (km)	Resistance (pu) values	R (ohms)	Reactance (pu) values	Reactance X (ohms)	L = X / (2*3.14*50)	Susceptance (pu) values	Susceptance B (siemens)	C = 1 / (B*2*3.14*50)
1 to 2	220	99.14	0.0123	0.060	0.0782	0.378488	0.001	0.146	0.70664	0.005
1 to 6	220	300	0.036	0.174	0.233	1.12772	0.004	0.445	2.1538	0.001
2 to 5	220	210	0.0257	0.124	0.165	0.7986	0.003	0.31	1.5004	0.002
3 to 4 (Line 1)	220	99.75	0.0124	0.060	0.0787	0.380908	0.001	0.147	0.71148	0.004
3 to 4 (Line 2)	220	99.75	0.0124	0.060	0.0787	0.380908	0.001	0.147	0.71148	0.004
4 to 5	220	210	0.0257	0.124	0.165	0.7986	0.003	0.31	1.5004	0.002
4 to 6	220	300	0.036	0.174	0.233	1.12772	0.004	0.445	2.1538	0.001
7 to 8 (Line 1)	400	500	0.0087	0.042	0.09	0.4356	0.001	3.152	15.25568	0.000
7 to 8 (Line 2)	400	500	0.0087	0.042	0.09	0.4356	0.001	3.152	15.25568	0.000

Note 1: Ractual = [Rpu*Vb^2]/Sb Note 2: Xactual = [Xpu*Vb^2]/Sb Note 3: Bactual = [Bpu*Vb^2]/Sb

Base MVA (Sb) = 100 MVA and Base Voltage (Vb) = 22 kV

Table B4: Transformer Data For CIGRE 12 Bus System

Transformer	Rating [MVA]	Nominal voltage of winding 1 [kV]	Nominal voltage of winding 2 [kV]	Tap ratio	Leakage reactance [pu]
7-1	1000	400	220	0.955	0.1
8-3	1000	400	220	0.955	0.1
2-10	600	220	22	1.05	0.1
3-11	250	220	22	1.05	0.1
1-9	100	220	22	1.05	0.01
6-12	200	220	33	1.045	0.1

The two generators (G2 and G3) have the same parameters expressed in pu based on their MVA rating. The parameters are given in Table B5.

Table B5: Parameters of Generators (G2 and G3).

Parameter	Tdo′	Xp	Xa	Xd	Xd′	Ra	Xd″
Value	8 s	0.2	0.2	1.8	0.3	0.0025	0.25
Parameter	Tdo″	Xq	Xq′	Tqo′	Xq″		Tqo″
Value	0.003 s	1.7	0.55	0.4s	0.25		0.003 s

Saturation curve: (0.5, 0.5), (0.8, 0.79), (1.0, 0.947), (1.2, 1.07), (1.5, 1.2) Inertia constant H=4 sec. The two generators G2 and G3 have AVR of type ST1A with independent supply. In addition, generator G2 had PSS of type PSS1A using shaft speed as its input signal.

Table B5: Automatic Voltage Regulator (AVR) and Power System Stabilizer (PSS).

AVR Parameter	**Value**
Lead time constant Tc	1 Sec.
Lag time constant Tb	10 Sec.
Gain Ka	200
Exciter maximum (upper) limit Vrmax	7
Exciter minimum (lower) limit Vrmin	0.6
PSS parameter	Value
1st lead time constant T1	0.15 Sec.
2nd lead time constant T1	0.15 Sec.
1st lag time constant T2	0.04 Sec.
2nd lag time constant T4	0.04 Sec.
Washout time constant T5	10 Sec.

Appendix C: The calculation of constant current source value used in farm side for Model-1

It is considered that system power is $P = 100\ \text{MW}$ (given data); The Farm Side Phase Voltage= $V = 132\ \text{kV}$ (given data) ; therefore a single phase current value is calculated as in Eq. (C.1).

$$P = 3 \times I \times V \quad , \quad 100 \times 10^{6} = 3 \times 132 \times 10^{3} \times I \qquad \text{(C.1)}$$

$I = 252.5$ A and hence, the constant current source amplitude is used as 252.5 A in the farm side.

Appendix D: Design of the PI controllers for Matlab Simulink Model-1

Design of inner current control loop: In order to design a PI controller for the d and q current controller loop, it is assumed that the closed loop current natural frequency is $\omega_n = 200$ Hz because the inner control loop is 10 times faster than the outer control loop; and the damping factor is $\xi = 0.8$ [47]. It is considered that the grid side inductance value is $L = 0.001$ H. It is assumed that there are no power losses in the converter, therefore grid side resistance is negligible in this design. The PI controller calculation is given as below:

The plant is shown as; hence Plant $G(s) = \frac{1}{sL} = \frac{1}{0.001s} = \frac{1000}{s}$; PI controller $G_c(s) = \frac{k(s+a)}{s}$.

Closed Loop Transfer Function: $1 + G(s).G_c(s) = 1 + \frac{k(s+a)}{s}.\frac{1000}{s} = 0$ With respect to the plant, $s^2 + 1000ks + 1000ka = 0$. The Characteristic equation of Closed Loop Transfer Function is $s^2 + 2\xi\omega_n + \omega_n{}^2 = 0$. Where $\omega_n = 2\pi f = 2\pi.200Hz = 1256.6rad/s$ and $\xi = 0.8$. $s^2 + 2\xi\omega_n + \omega_n{}^2 = s^2 + 2010.5s + 1579043.5 = 0$, Both of the equation should be equal, therefore; $s^2 + 1000ks + 1000ka = s^2 + 2010.5s + 1579043.5$ while $k = 2$ and $a = 785.6$ are obtained from this result. Therefore, **PI controller =** $\frac{2(s+789.5)}{s}$

Design of Outer Voltage Control Loop: In order to design a PI controller for the d and q voltage controller loop, it is assumed that the closed loop voltage natural frequency is $\omega n = 20Hz$ because the outer control loop is 10 times slower than the inner control loop and damping factor is $\xi = 0.8$

[47]. It is considered that DC-link capacitance value is $C = 0.0001F$. The PI controller calculation is given as: Plant $G(s) = \frac{1}{sC} = \frac{1}{0.0001s} = \frac{10000}{s}$; and PI controller $G_c(s) = \frac{k(s+a)}{s}$.

Closed Loop Transfer Function: $1 + G(s).G_c(s) = 1 + \frac{k(s+a)}{s}.\frac{10000}{s} = 0,$ with respect to the plant, $s^2 + 10000ks + 10000ka = 0$. The Characteristic equation of Closed Loop Transfer Function is $s^2 + 2\xi\omega_n + \omega_n{}^2 = 0$. Where $\omega_n = 2\pi f = 2\pi.20Hz = 125.66rad/s$ and $\xi = 0.8$ $s^2 + 2\xi\omega_n + \omega_n{}^2 = s^2 + 200.1s + 15775.3 = 0$. Both of the equation should be equal, therefore; $s^2 + 10000ks + 10000ka = s^2 + 201s + 15790.5$, while $k = 0.02$ and $a = 78.8$ are obtained from this result, therefore **PI controller=** $\frac{0.02(s+78.8)}{s}$.

Appendix E: The calculation of the DC Voltage and the DC link Capacitance for Matlab Simulink Model-2

According to given data, the RMS Grid phase voltage is 132 kV and therefore the peak grid voltage is; $V_{peak} = \sqrt{2} \times V_{rms} = \sqrt{2} \times 132000 = 186676.2$ V. It is assumed that modulation index is $M = 0.8$. The DC link voltage Vdc is calculated as in Eq. (E.1):

$$Vdc = \frac{2 \times Vac}{M} = \frac{2 \times 132000}{0.8} = 330000V \qquad \text{(E.1)}$$

The required capacitor size is calculated as in Eq. (E.2) [31]. Where E is energy and it is assumed that $\tau = 1$ second and so power is converted to energy as in Eq. (E.2).

$$E = \frac{1}{2} \times C \times Vdc^2$$

$$E = P \times \tau = 100MW \times 1s = 100MJ \qquad \text{(E.2)}$$

$$C = \frac{2 \times E}{Vdc^2} = \frac{2 \times 100 \times 10^6}{330000^2} = 1.83 \times 10^{-3} F$$

But it should be noted that this capacitor value is not suitable for the HVDC Link with the attached average value model of the DFIG based wind farm. The theoretical result of the DC link capacitor value is obtained as $1.83 \times 10^{-3} F$ but for the practical situation, this value is not suitable. Therefore, in this HVDC system, the DC link capacitor value is chosen as $0.1\,\text{F}$. Now, the expected simulation results are obtained from the design.

Appendix F: Design of the PI controllers for Matlab Simulink Model-2

Design of inner current control loop: In order to design a PI controller for the d and q current controller loop, it is assumed that the closed loop current natural frequency is $\omega n = 200Hz$ because the inner control loop is 10 times faster than the outer control loop; and the damping factor is $\xi = 0.8$ [47]. It is considered that the grid side inductance value is $L = 0.001H$. It is assumed that there are no power losses in the converter, therefore grid side resistance is negligible in this design. The PI controller calculation is given as below:

The plant is shown as; hence Plant $G(s) = \frac{1}{sL} = \frac{1}{0.001s} = \frac{1000}{s}$; PI controller $G_c(s) = \frac{k(s+a)}{s}$

Closed Loop Transfer Function: $1 + G(s).G_c(s) = 1 + \frac{k(s+a)}{s}.\frac{1000}{s} = 0$, with respect to the plant, $s^2 + 1000ks + 1000ka = 0$, The Characteristic equation of Closed Loop Transfer Function is $s^2 + 2\xi\omega_n + \omega_n{}^2 = 0$, where $\omega_n = 2\pi f = 2\pi.200Hz = 1256.6rad/s$ and $\xi = 0.8$.

$s^2 + 2\xi\omega_n + \omega_n{}^2 = s^2 + 2010.5s + 1579043.5 = 0$. Both of the equation should be equal, therefore; $s^2 + 1000ks + 1000ka = s^2 + 2010.5s + 1579043.5$, $k = 2$ and $a = 785.6$ are obtained from this result. Therefore, **PI controller =** $\frac{2(s + 785.6)}{s}$.

Design of Outer Voltage Control Loop: In order to design a PI controller for the d and q voltage controller loop, it is assumed that the closed loop voltage natural frequency is $\omega n = 20Hz$ because the outer control loop is 10 times slower than the inner control loop and damping factor is $\xi = 0.8$ [47]. It is considered that DC-link capacitance value is $C = 0.1$ F. The PI controller calculation is given as below:

Plant $G(s) = \frac{1}{sC} = \frac{1}{0.1s} = \frac{10}{s}$; PI controller $G_c(s) = \frac{k(s + a)}{s}$, Closed Loop Transfer Function: $1 + G(s).G_c(s) = 1 + \frac{k(s + a)}{s}.\frac{10}{s} = 0$, with respect to the plant, $s^2 + 10ks + 10ka = 0$

The Characteristic equation of Closed Loop Transfer Function is $s^2 + 2\xi\omega_n + \omega_n{}^2 = 0$. Where $\omega_n = 2\pi f = 2\pi.20Hz = 125.66rad/s$ $\xi = 0.8$ $s^2 + 2\xi\omega_n + \omega_n{}^2 = s^2 + 200.1s + 15775.3 = 0$,

Both of the equation should be equal, therefore; $s^2 + 10ks + 10ka = s^2 + 201s + 15790.5$, $k = 20$ and $a = 79$ are obtained from this result, therefore, **PI controller=** $\frac{20(s + 79)}{s}$.